# OCEANIC THERMAL RESPONSE TO A TIME-DEPENDENT HURRICANE MODEL

Thomas Stewart Fraim

NAVAL POSTGRADUATE SCHOOL
Monterey, California

# THESIS

# OCEANIC THERMAL RESPONSE TO A TIME-DEPENDENT HURRICANE MODEL

by

Thomas Stewart Fraim

Thesis Advisor: R. L. Elsberry

September 1973

*Approved for public release; distribution unlimited.*

# Oceanic Thermal Response
# to a
# Time-Dependent Hurricane Model

by

Thomas Stewart Fraim
Lieutenant, United States Navy
B.S., University of Michigan, 1967

Submitted in partial fulfillment of the
requirements for the degree of

MASTER OF SCIENCE IN METEOROLOGY

from the

NAVAL POSTGRADUATE SCHOOL
September 1973

# ABSTRACT

A layer-ocean model was developed based on the mixed layer models of Kraus and Turner (1967) and Denman (1972). The ocean model was coupled to Pearson's (1972) time varying, symmetrical-stationary hurricane model which was based on a model proposed by Riehl (1963), and in which the air-sea interaction was specified by Cardone's (1969) extension of Blackadar's (1965) two-layer, baroclinic boundary-layer model. Time-dependent solutions for ocean mixed layer depth and temperature were obtained in response to interaction with the atmospheric model. Solutions indicated that the interaction between entrainment mixing and upwelling was most important in changing mixed-layer depth and temperature. Radiational effects, internal waves, turbulent scale energy dissipation, and large-scale ocean currents were not included in the present ocean model.

# TABLE OF CONTENTS

# LIST OF TABLES

# LIST OF FIGURES

# ACKNOWLEDGEMENTS

The author wishes to express his sincere gratitude to Dr. R. L. Elsberry for his invaluable guidance and Dr. R. L. Haney for his constructive comments as second reader.

Appreciation is also expressed to the W. R. Church Computer Center Facility of the Naval Postgraduate School.

# I. INTRODUCTION

It is widely accepted that the source region for the hurricane heat engine is the underlying ocean. Although the ocean is virtually an infinite heat source, it is generally accepted that sea-surface temperatures in excess of 26C are necessary for forming and maintaining a mature hurricane. At the same time the ocean acts as a sink for the hurricane's momentum which is imparted to the ocean through surface stress. It is the balance of these two processes which was the basis for Riehl's (1963) steady-state hurricane model in which the tangential wind profile, outside the radius of maximum winds, was specified as $v_\theta r^{1/2}$ = constant.

Corgnati (1971) adopted Riehl's work to develop a model which used boundary-layer predictive equations for moisture and temperature, and bulk aerodynamic equations for the fluxes at the air-sea interface. Corgnati included a fairly simple ocean model which described the oceanic response to convective mixing as a result of heat extraction; however, most experiments were run with constant sea surface temperatures.

Pearson (1972) modified Corgnati's model by using Cardone's (1969) extension of Blackadar's (1965) two-layer near-neutral, baroclinic boundary-layer model to

calculate the fluxes at the air-sea interface. Pearson's model produced steady-state solutions for constant sea-surface temperatures, and exhibited greater sensitivity to these temperatures than did the Corgnati model.

It was felt that to more realistically describe the hurricane-ocean interaction, a more complex ocean model incorporating wind mixing, convective mixing, and advection, was required. It was the object of this study to develop such a model and couple it to Pearson's atmospheric model through the boundary-layer fluxes of heat and momentum. The current ocean model is based on mixed-layer models of Kraus and Turner (1967), which predicts the mixed-layer temperature and depth in response to wind mixing and convection, and Denman (1972), which includes the effect of upwelling. It was hoped that the ocean model may help to explain which of the mechanisms is of greatest importance in producing the areas of low sea-surface temperatures observed in the wake of hurricanes. Investigators have attributed the low temperatures to various mechanisms with little agreement as to which is the most important. For example, Jordan (1964) concluded that mixing was the more important factor. Fischer (1958) considered upwelling to be the most important. Leipper (1967) concluded that upwelling, produced by surface divergence, was the most important near the hurricane's center and that mechanical mixing dominated at larger radii.

The present ocean model was run using each of the three cooling mechanisms (convection, wind mixing, and advection), separately and in various combinations, in an attempt to study their relative effects upon the ocean upper thermal structure and subsequent heat content.

# II. DESCRIPTION OF THE MODEL

## A. ATMOSPHERIC VORTEX

Riehl (1963), in his early work, assumed conservation of potential vorticity in the inflow layer and a bulk aerodynamic equation for surface stress with constant drag coefficient and inflow angle, to derive the relation

$$v_\theta r^{1/2} = \text{constant} \qquad (1)$$

which specifies the radial profile of cyclonic tangential winds at the top of the atmospheric boundary layer as shown in Figure (1). The outer limit of the circulation described by Riehl's model was defined by the radius ($r_o$) at which the cyclonic flow becomes anticyclonic in the outflow layer. Riehl assumed that the air ascending in the eye-wall region, and flowing cyclonically outward aloft, conserves absolute angular momentum. With this assumption, one obtains

$$r_o = \left(\frac{2}{f} v_{\theta_i} r_i\right)^{1/2} \qquad (2)$$

where f is the Coriolis parameter and the i subscripts denote values at the radius of maximum wind speed. The present atmospheric model assumed that the radius of maximum wind ($r_i$) was coincident with the eye-wall radius. Since the eye wall is a preferred region for deep convection and latent heat release in observed hurricanes,

those boundary-layer air parcels with the greatest heat and moisture content in the model were assumed to be at the eye wall. Thus, $r_i$ was taken to be the radius at which the equivalent potential temperature ($\theta_e$), averaged over five grid increments ($\Delta r$ = 3km), was a maximum. Between the vortex center and $r_i$ the winds were assumed to obey $v_\theta r^{-1}$ = constant, which agreed with data from Riehl (1963), as well as Shea and Gray (1972).

From observations, Riehl developed the relationship

$$P' = -2.56\ \theta_e' \tag{3}$$

where P' is the pressure departure from 1005 mb and $\theta_e'$ is the equivalent potential temperature departure from 350 K. It was assumed that the atmospheric vortex was in a state of quasi-equilibrium with the boundary layer fluxes of heat and moisture, which determined the increase in $\theta_e'$ and thereby P' of the inflowing air.

Assuming a gradient balance between the wind and pressure field

$$\frac{1}{\rho}\frac{\partial P}{\partial r} = \frac{v_\theta^2}{r} + f\ v_\theta \tag{4}$$

and using the relation

$$v_\theta^2 = \frac{v_{\theta_i}^2\ r_i}{r}\ ; \tag{5}$$

integration of (4) from $r_o$ to $r_i$, yields the following expression for the maximum wind speed:

$$\begin{aligned} v_{\theta_i} &= \frac{0.5 r_o}{r_o - r_i} \Big[ -2f\sqrt{r_i r_o} - r_i \\ &+ \sqrt{4f^2(\sqrt{r_i r_o} - r_i)^2 + 10^6 \frac{r_o - r_i}{\rho r_o} (\theta_{e_i} - \theta_{e_o})} \Big] \end{aligned} \qquad (6)$$

For the symmetric model, the time-dependent predictive equations for potential temperature ($\theta$) and specific humidity (q), which characterize the boundary-layer properties through a specified depth ($\Delta P$), are

$$\frac{\partial \theta}{\partial t} = - \frac{\partial (r v_r \theta)}{r\ \partial r} - \frac{\partial (\omega \theta)}{\partial P} + \frac{g Q_S}{C_p \Delta P}\ , \text{ and} \qquad (7)$$

$$\frac{\partial q}{\partial t} = - \frac{\partial (r v_r q)}{r\ \partial r} - \frac{\partial (\omega q)}{\partial P} + \frac{g Q_E}{L \Delta P} \qquad (8)$$

where ($Q_S$) and ($Q_E$) are the oceanic sensible and latent heat fluxes, respectively. $C_p$ and L are the specific heat and latent heat of vaporization. Radial ($v_r$) and vertical ($\omega$) components of motion are related through the continuity equation

$$\frac{\partial \omega}{\partial P} = - \frac{\partial (r v_r)}{r\ \partial r}\ . \qquad (9)$$

The surface fluxes $Q_S$, $Q_E$, $\tau_{\theta_s}$, and the integrated radial motion ($v_r$) are determined from the boundary-layer model.

## B. BOUNDARY-LAYER MODEL

Following Pearson (1972), the boundary-layer model was a two-layer, baroclinic model developed by Cardone (1969) as shown in Figure (2). The Cardone model of the marine boundary layer was an extension of the near-neutral, fixed-terrain model described by Blackadar (1965). The model used the $v_\theta$ profile from the atmospheric vortex model, together with a computed boundary-layer thermal wind and made use of Monin-Obuhkov similarity theory and stationary Ekman-layer theory to calculate the friction velocity $u_*$, the stability index $L_*$, and the inflow angle $\alpha$. These are then used to calculate a vertical mean radial wind, $\bar{u}$, within the surface layer from

$$\bar{u} = \left\{ \sum_{i=1}^{4} \frac{u_*}{K} [\mathrm{Ln} \frac{Z_i}{Z_o} - \psi(L_*)] \right\} /4 \qquad (10)$$

and the total heat flux (H) from

$$H = Q_S + Q_E = [-u_*^3 C_p \rho a_h \bar{\theta}]/KgL' \qquad (11)$$

where $u_*$ = friction velocity, $(\tau/\rho)^{1/2}$, where $\tau$ is the radial stress component,

$Z_o = \dfrac{6.84 \times 10^{-5}}{u_*} + 4.28 \times 10^{-3}\, u_*^2 - 4.43 \times 10^{-4}$, surface roughness (m),

$\psi(L_*)$ = wind profile function [Cardone (1969)],

$L = Z/L'$, stability index,

$Z_i$ = heights in the surface layer,

$K$ = von Karman constant,

$\overline{\theta}$ = mean potential temperature in the boundary layer, and

$a_h = K_h/K_m$, ratio of heat transfer coefficient to turbulent transfer coefficient for momentum.

The individual $Q_s$ amd $Q_E$ fluxes were specified according to the Bowen ratio $C_p(\theta_a - Q_w)/L_v(q_a - q_w)$. The radial wind within the spiral layer was determined through integration of the Ekman solution to get

$$\int_h^{\infty} v_r dZ = \sqrt{2}\, v_\theta \sin \alpha \frac{e^{-Bh}}{2Bh}\left[\cos\left(\alpha + \frac{3\pi}{4} - Bh\right) - \sin\left(\alpha + \frac{3\pi}{4} - Bh\right)\right] \qquad (12)$$

where

$$B = (f/2u_* Kh)^{1/2}$$

To include the centripetal acceleration, the Coriolis parameter (f) was replaced by $(f + \frac{v_\theta}{r})$. The values of $v_r$ in the surface layer (Equation 10) and Ekman layer (Equation 12) were then used in determining the vertical motion (Equation 9) and the advection of heat and moisture [Equations (7) and (8)] in the prediction portion of the model.

## C. OCEAN MODEL

### 1. Description

In an attempt to more realistically describe the air-sea interaction associated with a time-varying

hurricane model, it was decided to develop an ocean model capable of producing time-varying solutions of mixed-layer depth and temperature in response to atmospheric forcing. Previously the hurricane model produced time-varying solutions for constant sea-surface temperatures until a steady state was reached.

The present ocean model was initialized with sea-surface temperature ($T_s$), mixed-layer depth ($h_o$), below layer gradient ($\partial T/\partial Z$), and deep-layer temperature ($T_d$) as shown in Figure (3). By allowing the ocean thermal structure to change, it was hoped that a more thorough understanding of the air-sea interaction process might be possible. The present model is designed for a wind-dominated region where there is negligible downward heat flux, either by solar radiation or sensible and latent heat (condensation) fluxes from the atmosphere to the ocean. In the absence of upwelling this precludes any possibility for a decreasing mixed-layer depth. The atmospheric forcing of the ocean model was by surface kinetic energy input (wind stress) and upward sensible and latent heat (evaporation) fluxes. Both wind stress and heat flux produced changes in mixed-layer depth and temperature, surface stress by entrainment mixing and the heat fluxes by convective mixing. The entrainment mixing was caused by surface generated turbulent motions at the depth of the mixed-layer interface.

A partitioning procedure was used to budget the total atmospheric stress ($\tau_a$) between surface turbulence production and generation of a radial mass transport according to Ekman theory. The effects of entrainment mixing (turbulence) were assumed to be redistributed uniformly throughout the layer by turbulent diffusion. A radial wind-driven current was computed from the mass transport and, by employing the continuity equation, areas of upwelling and downwelling were calculated. Thus, the ocean model incorporated the primary mechanisms believed to produce the observed ocean cooling in the wake of hurricanes. Internal waves, large-scale currents, and turbulent-scale energy dissipation within the mixed layer were not included. At six-hour intervals the ocean heat content was computed and compared to the initial values as a check on the model's solution of mixed-layer depth and temperature.

The time-dependent mixed-layer temperatures generated by the ocean model produced variations in the atmospheric model's $v_\theta$ profile, which in turn produced variations in the atmospheric forcing (surface stress and heat fluxes). This tended to bring the coupled models into a quasi-steady state condition in all cases except ones in which advection was included.

## 2. Mathematical Development of Ocean Model

By neglecting molecular heat fluxes and viscous generation of heat, Denman (1972) wrote the first law

of thermodynamics (conservation of thermal energy) for an incompressible fluid in the following form:

$$\frac{dT}{dt} = \frac{Q_T}{\rho_w C_p} \tag{13}$$

where

$Q_T = \gamma R_* e^{-\gamma Z}$, specifies the heat source term, (14)

$\rho_w$ = ocean water density,

$\gamma$ = average extinction coefficient,

$C_p$ = specific heat at constant pressure,

$R_*$ = solar radiation incident on the sea surface, and

$Z$ = depth in the ocean, positive downward.

Substitution of (14) into (13) gives the first law in the form

$$\frac{dT}{dt} = \gamma R e^{-\gamma Z} \tag{15}$$

where $R = R_*/\rho C_p$

The total derivative was expanded in flux form and (15) was written in time-averaged turbulent form:

$$\frac{\partial \bar{T}}{\partial t} + \frac{1}{r}\frac{\partial(\bar{u}_r r \bar{T})}{\partial r} + \frac{\partial(\bar{w}\ \bar{T})}{\partial Z} + \frac{\partial(\overline{w'T'})}{\partial Z} = \gamma R e^{-\gamma Z} \tag{16}$$

or

$$\frac{d\bar{T}}{dt} = \gamma R e^{-\gamma Z} - \frac{\partial(\overline{w'T'})}{\partial Z} \tag{17}$$

where $\bar{u}_r$ = vertical average radial velocity in the mixed layer, and $T$, $u_r$ and $w$ were replaced by $\bar{T} + T'$, $\bar{u}_r + u'_r$,

and $\bar{w} + w'$, respectively. The term involving $(\overline{u_r'T'})$ in Equation (16) was dropped because it was assumed that there was no systematic correlation between u' and T'. Equation (17) is the heat conservation equation where $\partial(\overline{w'T'})/\partial Z$ represents the local divergence of the turbulent vertical heat flux. It was this term which redistributed the heat exchanged at the boundaries uniformly throughout the homogeneous mixed layer. At the ocean surface, the downward turbulent heat flux, $(\overline{w'T'})_o$, was equal to the nonradiative heat transfer through the ocean surface, i.e.,

$$(\overline{w'T'})_o = -(Q_E + Q_S)/\rho_w C_p \tag{18}$$

where $Q_E$ and $Q_S$ were the upward latent and sensible heat fluxes, respectively, computed in the boundary-layer model. At the bottom of the mixed layer, the downward turbulent heat flux was equal to the heat transfer through the interface due to entrainment mixing, i.e.,

$$(\overline{w'T'})_{h_o} = \left(\frac{dh_o}{dt} - \bar{w}\right)(T_S - T_h) \tag{19}$$

where $\frac{dh_o}{dt}$ = time variation of mixed-layer depth,

$\bar{w}$ = vertical advection velocity at depth $(h_o)$,

$T_S$ = mixed-layer temperature, and

$T_h$ = temperature at a finite depth below mixed-layer depth.

For entrainment mixing, the turbulent flux $(\overline{w'T'})_{h_o}$ was positive which corresponds to warm water ($T' > 0$) being

forced downward ($w' > 0$) and cold water ($T' < 0$) being lifted upward ($w' < 0$). This process was accomplished against buoyancy forces by the kinetic energy input at the surface and the potential to kinetic energy conversion by convective overturning.

Integrating Equation (17) over the depth of the mixed layer ($h_o$) and replacing the boundary turbulent heat fluxes by Equations (18) and (19), yields a thermal energy equation for the mixed layer,

$$\frac{dT_S}{dt} h_o = R(1-e^{-\gamma h}) - (Q_E+Q_S)/\rho_w C_p - \left(\frac{dh}{dt} - w\right)(T_S - T_h) \qquad (20)$$

By expanding the total derivatives in flux form and ignoring the radiation effects, (R), (20) becomes a predictive equation for the local change in the mixed-layer depth ($h_o$), i.e.,

$$\frac{\partial h_o}{\partial t} = \frac{-h_o}{(T_S - T_h)}\left[\frac{\partial \bar{T}_S}{\partial t} + \frac{1}{r}\frac{\partial(\bar{u}_r r \bar{T}_S)}{\partial r} + \frac{\partial(\bar{w}\,\bar{T}_S)}{\partial z}\right] - \frac{Q_E + Q_S}{\rho_w C_p (T_S - T_h)} - \bar{u}_r \frac{\partial h_o}{\partial r} + \bar{w} \; . \qquad (21)$$

To develop a corresponding equation for mixed-layer temperature changes, Denman (1972) integrated Equation (17) twice, once over a depth z and once over the depth of the mixed layer ($h_o$). The resulting expression,

$$\frac{d\bar{T}_S}{dt}\,\frac{h_o^2}{2} = -\,\frac{(Q_E + Q_S)}{\rho_w C_p}\,h_o - \int_o^{h_o} \overline{(w'T')}_Z \, dZ \qquad (22)$$

represents a mechanical energy equation for the mixed layer. The term $\int_o^{h_o} \overline{(w'T')}dZ$ specifies the conversion of potential energy into kinetic energy by convection within the mixed layer. If one considers the mechanical energy balance expression

$$W + G - D = 0 \qquad (23)$$

where G = kinetic input from the wind,

D = dissipation within the mixed layer, and

$W = -\int_o^{h_o} \overline{(w'T')}dZ$ (potential to kinetic energy conversion),

substitution of Equation (22) into (23) yields

$$\frac{d\bar{T}_S}{dt}\,\frac{h_o^2}{2} = -\,\frac{(Q_E + Q_S)}{\rho_w C_p}\,h_o - (G-D) \;. \qquad (24)$$

Expanding the total derivative of temperature in flux form and solving for the local temperature change yields

$$\frac{\partial \bar{T}_S}{\partial t} = -\,\frac{2(G-D)}{h_o^2} - \frac{2(Q_E - Q_S)}{h_o\,\rho_w C_p} - \frac{1}{r}\,\frac{\partial(\bar{u}_r r \bar{T}_S)}{\partial r} - \frac{\partial(\bar{w}\;\bar{T}_S)}{\partial Z} \qquad (25)$$

which is a mechanical energy equation specifying the change in mixed-layer temperature due to entrainment

mixing, convection, and advection. Equation (25) can be used to eliminate $\partial T_s/\partial t$ from the heat equation (21):

$$\frac{\partial h_o}{\partial t} = \frac{2(G-D)}{h_o(T_s-T_h)} + \frac{(Q_E+Q_S)}{\rho_w c_p(T_s-T_h)} - \bar{u}_r \frac{\partial h_o}{\partial r} + \bar{w} \qquad (26)$$

Equations (25) and (26) represent a system of two equations with three unknowns, $T_s$, $h_o$, and $T_h$ ($\bar{u}_r$ and $\bar{w}$ will be obtained from Ekman theory and the equation of continuity). To close this system therefore, a third equation or relation was required which specified changes in $T_h$ as being dependent upon changes in $h_o$. The parameter which imposed this dependency was the below-layer gradient $(\partial T/\partial Z)$ which was assumed to be uniformly affected by vertical velocities and thus remained constant. Time variations of $T_h$ were specified by the expression

$$\frac{\partial T_h}{\partial t} = -(\bar{w} - \frac{dh_o}{dt})(\frac{\partial T}{\partial t})_{h_o} \qquad (27)$$

where $\bar{w}$ = vertical advection velocity.

The solution for $T_h$, which represented the lower temperature of the entrained water, proved to be very crucial in the mixed-layer depth and temperature solutions. It was the temperature difference $(T_s - T_h)$ which imposed the primary retarding force against unlimited deepening. As time progressed the difference $(T_s - T_h)$ increased, forming an actual step in the temperature profile at the base of

the mixed layer. Because of the stable lapse-rate ($\partial T/\partial Z < 0$), upwelling ($w<0$) contributed to a lowering of $T_h$ and, hence, increased the difference ($T_s - T_h$). Thus, upwelling had the effect of retarding the tendency for mixed-layer deepening. At the same time upwelling ($w<0$) enhanced mixed-layer temperature changes by decreasing the layer thickness (Equation 26) so that the energy input and heat fluxes would have a greater effect (Equation 25). Thus, Equations (25) (26), and (27) formed a system for unknowns $h_o$, $T_s$, and $T_h$. Space and time derivatives in (25) and (26) were approximated by centered differences, except for the initial time step which used a forward difference. A forward step was also used every 17th time step (3 hours) to prevent diverging solutions. Forward time differences were used in (27). The difference forms of (26) and (27) were solved together for $h_o$ and $T_h$ using a first guess depth and temperature ($T_s$) from the previous time step. The first guess depth in (26) and (27) was increased by 0.05m increments until the difference between the right and left hand sides of the difference form of (26) was less than or equal to 0.1m. Using the new mixed-layer depth, mixed-layer temperature was calculated from (25).

The mechanical energy input (G), in the ocean predictive equations (25) and (26), was specified according to Kraus and Turner (1965) as

$$G = \frac{1}{g\alpha\rho_a} \left(\frac{\rho_a}{\rho_w}\right)^{3/2} u_*\tau_o \qquad (28)$$

where $g$ = gravitational acceleration,

$\alpha = \frac{1}{\rho_w} \frac{d\rho_w}{dT}$ , coefficient of expansion,

$\rho_a$ = air density,

$\rho_w$ = sea water density,

$u_*$ = atmospheric friction velocity, and

$\tau_o$ = atmospheric surface stress.

In the ocean model, surface stress ($\tau_o$) used for the energy input term (G) depended exponentially upon the ratio of the mixed-layer depth ($h_o$) and the roughness length ($Z_o$):

$$\tau_o = \tau_a \text{ EXP } \left(-\frac{h_o}{CZ_o}\right) \qquad (29)$$

where

$\tau_a$ = total stress available from boundary-layer model, and

C = an arbitrary constant.

For a given roughness length ($Z_o$), the function exp $\left(-\frac{h_o}{CZ_o}\right)$ specified the percentage of total stress ($\tau_a$), available for turbulence generation as a function of mixed-layer depth (Table I). The use of the above partitioning procedure was an attempt to budget the available energy between turbulence generation (G) and production of wind-driven currents in the ocean model. Experiments were run

with various values of C and compared to each other as well as to a run in which all the surface stress was utilized for turbulence generation. The dissipation, D, was set to zero in all experiments.

The radial velocity, $u_r$, which is needed to close the system, was calculated in accordance with Ekman theory which specifies a spiral layer to a depth ($Z_e$) where the current direction has reversed from its surface direction and the speed is exp ($-\pi$) of the surface speed. Below the Ekman layer it was assumed that the wind had no direct influence. According to Ekman the radial component of motion within the spiral layer was described by

$$u_r = \frac{(\tau_a - \tau_o)\cos\alpha}{\rho_w (2f\,\frac{\mu}{\rho_w})^{1/2}} \, \mathrm{EXP}(-BZ)[\cos(-BZ) - \sin(-BZ)] \qquad (30)$$

where $Z_e = \pi/B$, specifies the Ekman depth,

$B = [\frac{f}{2\mu/\rho_w}]^{1/2}$,

$f$ = coriolis parameter,

$\rho_w$ = sea water density,

$\mu$ = vertical eddy coefficient of viscosity,

$Z$ = depth, and

$\alpha$ = atmospheric inflow angle.

Integration of (30) over a specified Ekman depth ($Z_e$) yields an expression for the net mass transport in the radial direction for the Ekman layer,

$$M_r = \tau_\theta / f \qquad (31)$$

## TABLE I

Stress used for mixing ($\tau_o$) vs. mixed-layer depth as a % of total stress ($\tau_a$). $Z_o = 10^{-2}$ m, $C = 10^4$ and $5 \times 10^3$.

| Mixed layer Depth (m) | $\tau_o$ as % of $\tau_a$ ($C=10^4$) | $\tau_o$ as % of $\tau_a$ ($C=5\times 10^3$) |
|---|---|---|
| 5 | .95 | .90 |
| 10 | .90 | .82 |
| 20 | .82 | .67 |
| 30 | .74 | .55 |
| 40 | .67 | .45 |
| 50 | .61 | .37 |
| 60 | .55 | .30 |
| 70 | .50 | .25 |
| 80 | .45 | .20 |
| 90 | .41 | .17 |
| 100 | .37 | .14 |

where $\tau_\theta = (\tau_a - \tau_o)\cos\alpha$, tangential atmospheric surface stress.

This represents a radial mass transport per unit distance in the tangential direction. One can calculate a mean radial advection velocity $(\bar{u}_r)$ for the mixed layer from the relation

$$\bar{u}_r Z_e = M_r/\rho_w \; . \tag{32}$$

The mean radial $(\bar{u}_r)$ and vertical $(\bar{w})$ components of motion are related through the continuity equation

$$\frac{\partial(\rho_w\ w)}{\partial Z} = -\frac{1}{r}\,\frac{\partial(\rho_w\ \bar{u}_r\ r)}{\partial r} \tag{33}$$

Equation (33) was integrated over depth $(Z_e)$ using the boundary condition $w(z=0) = 0$, to obtain $\bar{w}$ at $Z_e$

$$\rho_w\ \bar{w} = -\frac{1}{r}\,\frac{\partial}{\partial r}\left(\frac{r\ \tau_\theta}{f}\right) \tag{34}$$

which was taken to be $\bar{w}$ at $h_o$. The probable occurrence of a return flow at some depth below the mixed layer was not included in the present ocean model. Thus, the only effect on the below-layer gradient $(\partial T/\partial Z)$ was that due to vertical velocities and, hence, the gradient remained constant.

As a check on the cooling processes (wind mixing, convective mixing, and advection), the initial ocean heat content (cals/cm$^2$) for a depth $Z_b$ = 130m was calculated based on the initial temperature profile (Figure 3). This

value was then compared to the heat content at each grid point, computed at 6-hour intervals. For convective mixing-only, with the kinetic energy input (G) and the advection velocities ($\bar{u}_r$ and $\bar{w}$) equal to zero, Equations (25) and (26) predicted excessive mixed-layer deepening and cooling. Also the final grid point heat contents did not reflect just the heat (H) lost to the atmosphere due to upward heat fluxes ($Q_E$ and $Q_S$). Hence, for this case the mixed-layer depth and temperature were specified by a thermal equilibrium problem using the following set of equations:

$$h_o T_s = h_o' \, (T_s' - Q\Delta t/\rho_w C_p h_o') + \Delta h \, \frac{T_s - T_s'}{2}$$

$$h_o = h_o' + \Delta h \qquad (35)$$

$$T_s = T_s' + \frac{\partial T}{\partial Z} \Delta h$$

where $h_o'$ = initial mixed-layer depth,

$T_s'$ = initial mixed-layer temperature,

$\partial T/\partial Z$ = below-layer gradient,

$Q = Q_E + Q_S$, total upward heat flux,

$\rho_w$ = sea water density,

$\Delta t$ = time step (sec), and

$C_p$ = specific heat

For convective mixing only, equations (35) were solved at each time step for the change in mixed-layer depth ($\Delta h$). With this calculated depth change, the new layer depth ($h_o$) and temperature ($T_s$) were specified.

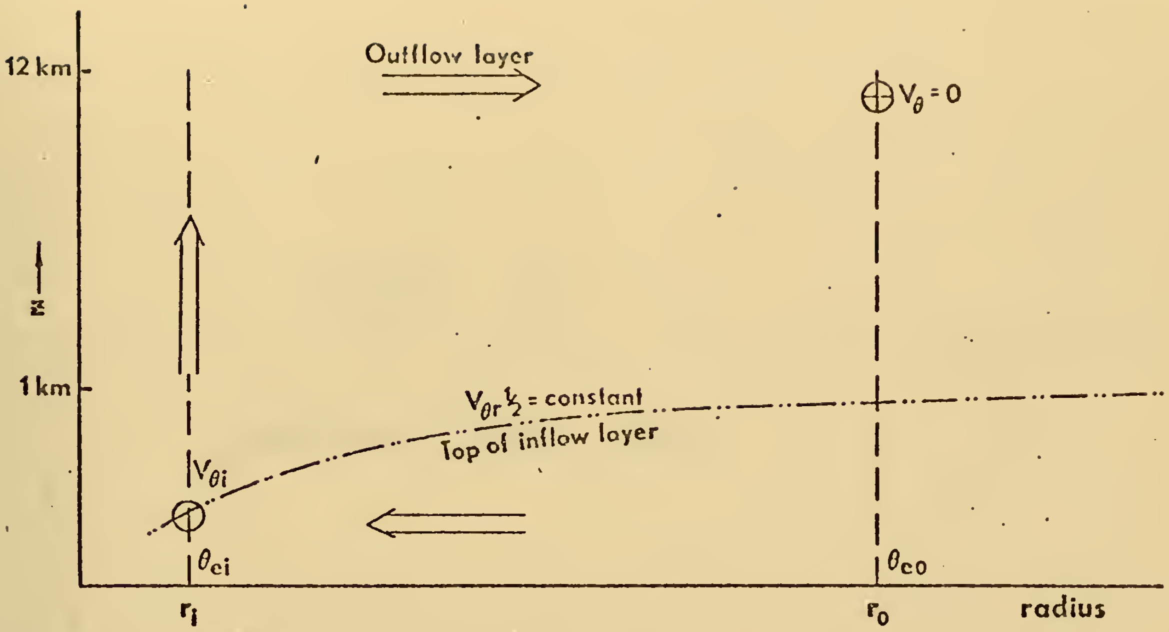

Figure 1. Atmospheric vortex model.

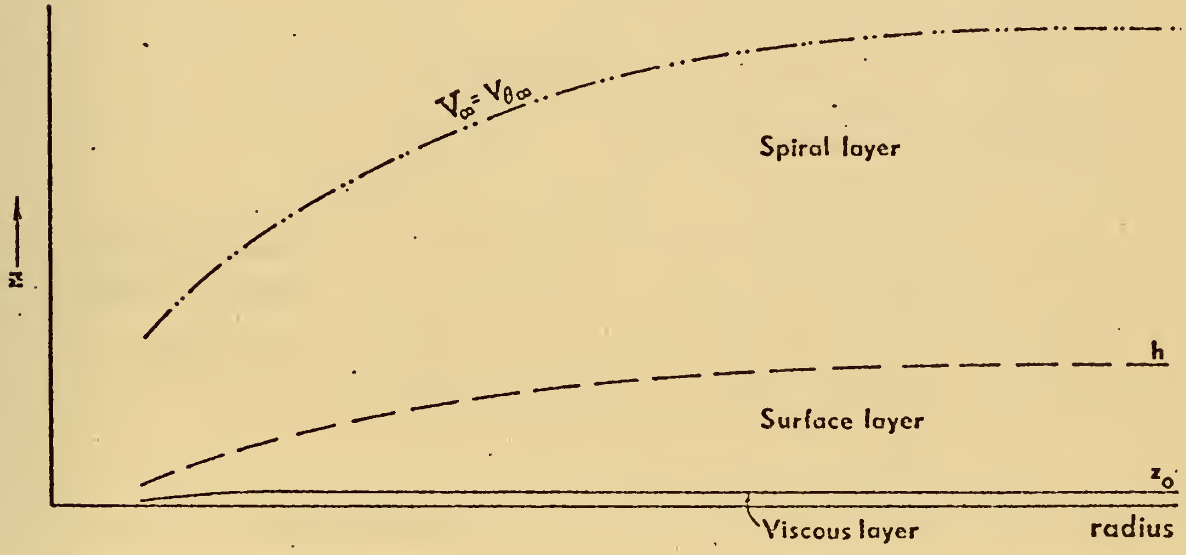

Figure 2. Boundary layer model.

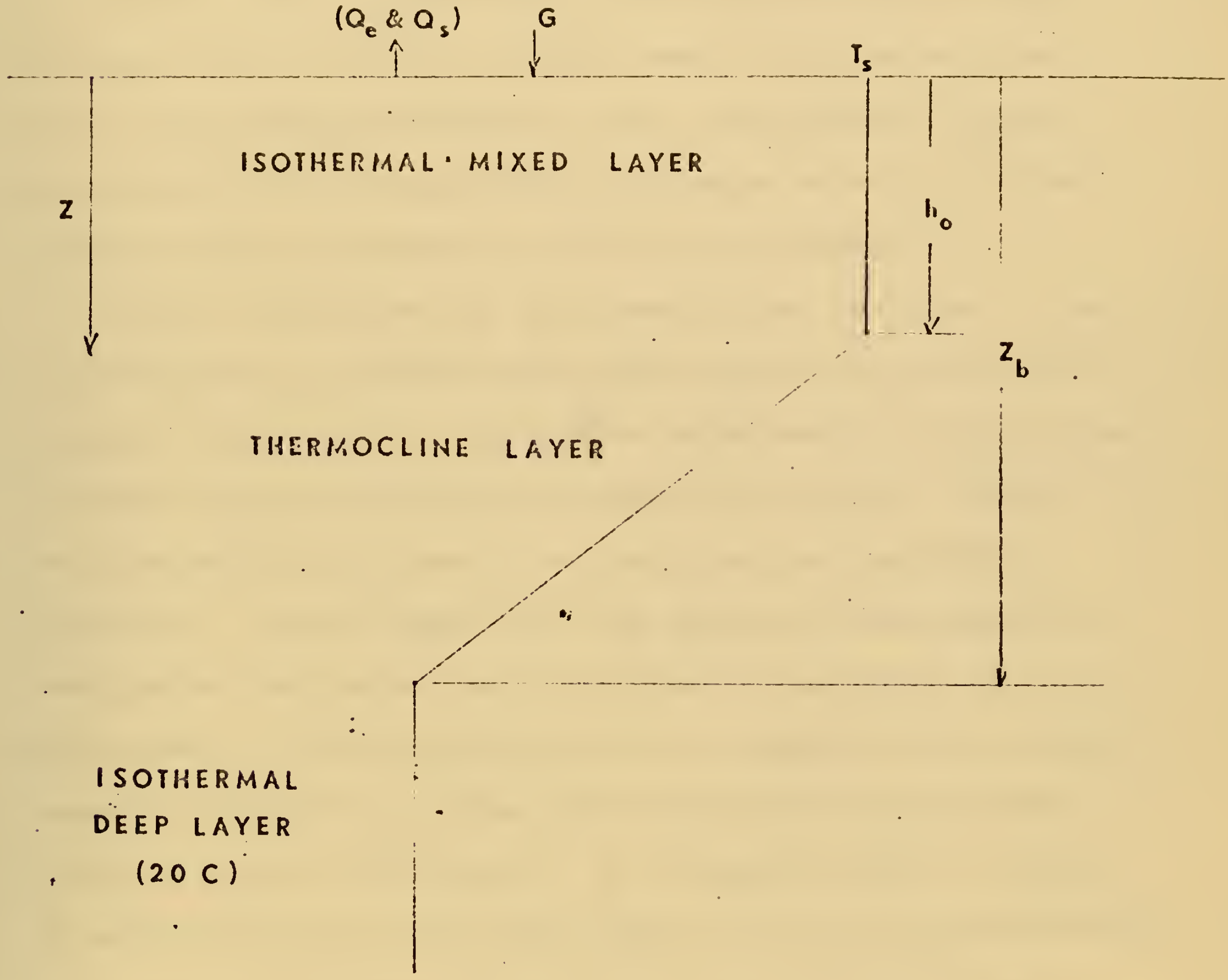

Figure 3. Ocean model.

## III. DISCUSSION OF RESULTS

As stated previously, the object of this study was to develop an ocean model capable of producing time-dependent solutions for mixed-layer depth and temperature in response to forcing from a symmetrical, stationary hurricane model. Previous work with the hurricane model was done with constant sea-surface temperatures and, consequently, little was learned of the ocean thermal changes or of the corresponding changes produced in the hurricane model.

In this investigation three mechanisms believed to contribute most in changing the ocean thermal structure were isolated and studied. These were entrainment mixing across a stable layer (wind stress), convective mixing (latent and sensible heat fluxes), and vertical and horizontal advection. It was hoped that the combined time-dependent, atmosphere-ocean model would help determine which of these mechanisms, either acting alone or in combination, was most important in producing the cold sea-surface temperatures observed beneath hurricanes. To accomplish this, a series of experiments were run using each of the cooling mechanisms alone and in combination with each other. Figures (4) through (32) depict radial profiles of various ocean parameters for the different experiments. For these runs the ocean model was initialized with mixed-layer depth of

30 meters, mixed-layer temperature of 30C, below-layer gradient of 10C/100m, and deep-layer temperature of 20C. The lower boundary of the model was fixed at 130 meters (Figure 3), below which there were assumed to be no thermal effects. Other initial temperature profiles can be used; however, the above values were believed to be fairly representative of the tropical ocean regions. The atmospheric model was initialized with air temperature of 29C, radius of maximum wind ($r_i$ = 27km), and maximum wind ($v_{\theta_i}$ = 30m/sec). In runs with various constant sea-surface temperatures, Pearson (1972) found a steady-state $v_{\theta_i}$ of 60m/sec for 30C.

The value of the constant (C) in the wind stress partitioning equation (29) was arbitrary fixed at $10^4$ in all the initial runs except the advection-only case. For this run the partitioning process was not used; consequently, all the available stress ($\tau_a$) was used to produce radial wind-driven currents ($\bar{u}_r$) and vertical velocities ($\bar{w}$). Since the partitioning process was an important assumption in the model, an entrainment-convection-advection experiment was run with a value of $5 \times 10^3$ for the constant (C) in Equation (29). With a smaller value of C, Equation (29) partitioned more atmospheric stress to producing ocean currents and less to entrainment mixing at all mixed-layer depths (Table I). An entrainment-convection run was also made in which the partitioning process was not used, hence

all available stress from the boundary-layer model was used in the kinetic energy term (G) in the mixed-layer depth and temperature predictive Equations [(25) and (26)].

## A. CONVECTIVE MIXING ONLY

For the convective mixing-only case, Equations (35) were solved for the mixed-layer depth (Figure 4) and temperature (Figure 5). The atmospheric forcing was by latent and sensible heat fluxes from the ocean surface to the atmosphere as computed in the boundary-layer model. Maximum cooling (0.5C) and deepening (5 meters) of the mixed layer at 18 hours occurred under the region of maximum wind ($r_i$) as expected from Equation (11) which relates total oceanic heat loss (H) to the cube of the friction velocity ($u_*$). Oceanic heat loss computed from initial and final temperature-depth profiles (Figure 6) in the ocean model compared quite favorably with the total heat extraction (H) computed in the boundary-layer model (Figure 7). The amount of ocean cooling due to convection was comparable to Jordan's (1964) estimates.

## B. ENTRAINMENT MIXING

Radial profiles of mixed-layer depth and temperature due only to entrainment mixing (Figures 8 and 9) were obtained by iterative solutions of Equations (25), (26), and (27). There was no ocean current generation in this run, and the partitioned stress (29), with $C = 10^4$, was

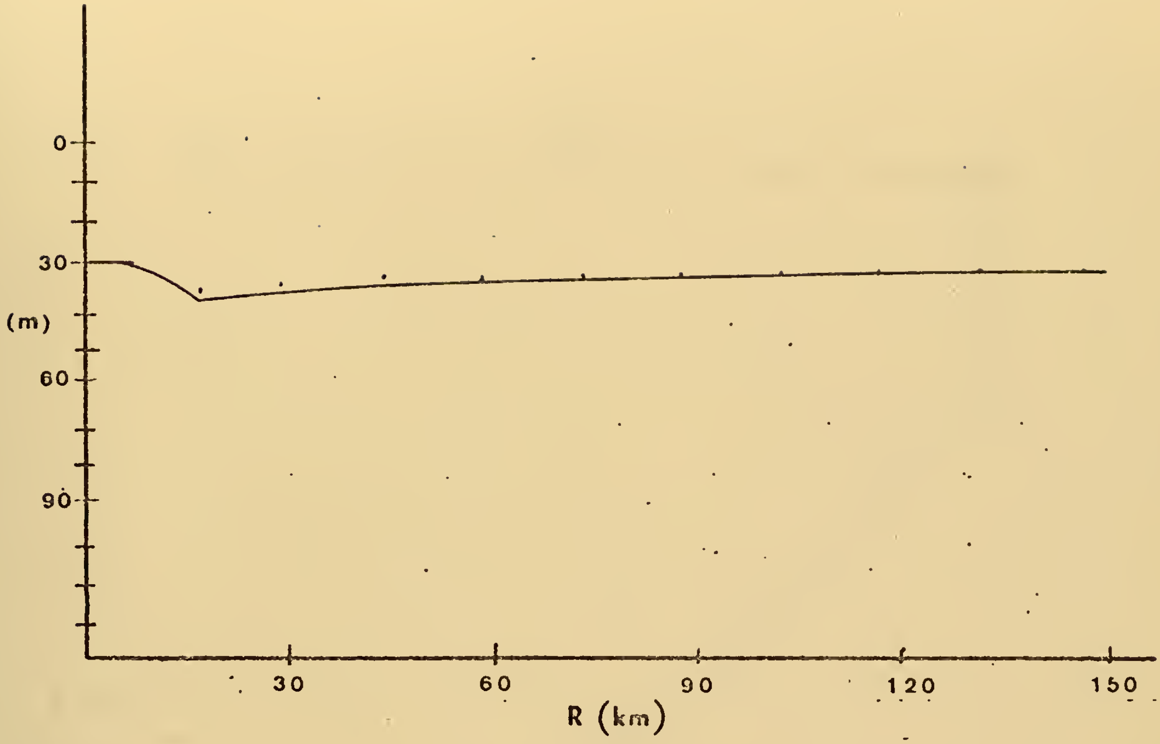

Figure 4. Radial profile of mixed-layer depth at 18 hours due to convective mixing.

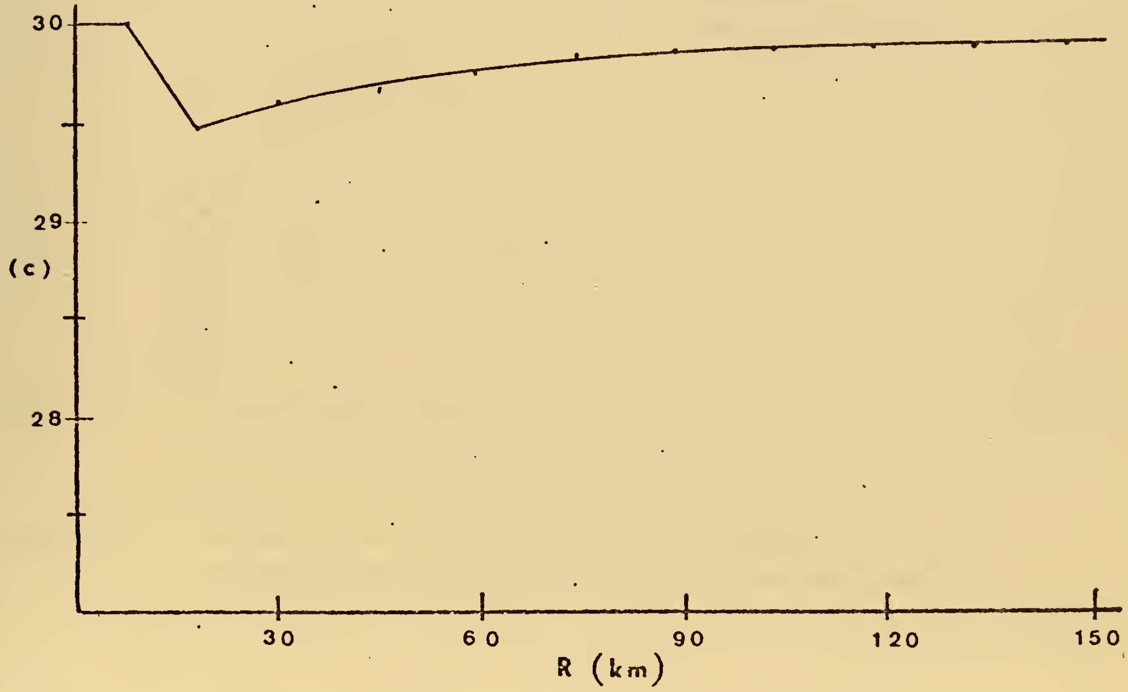

Figure 5. Same as Figure 4 except mixed-layer temperature.

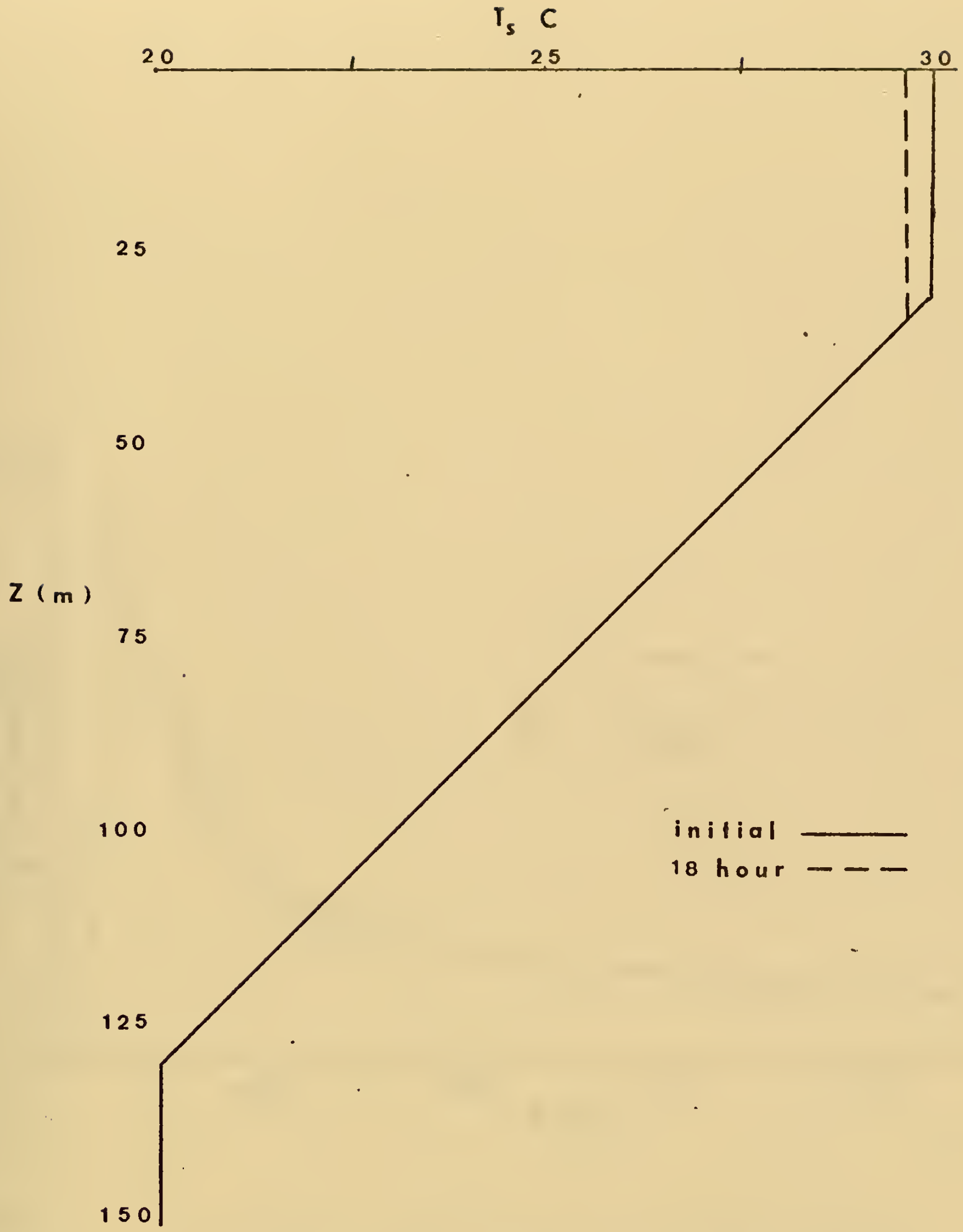

Figure 6. Predicted 18-hour vertical temperature profile at 30 km for convective mixing.

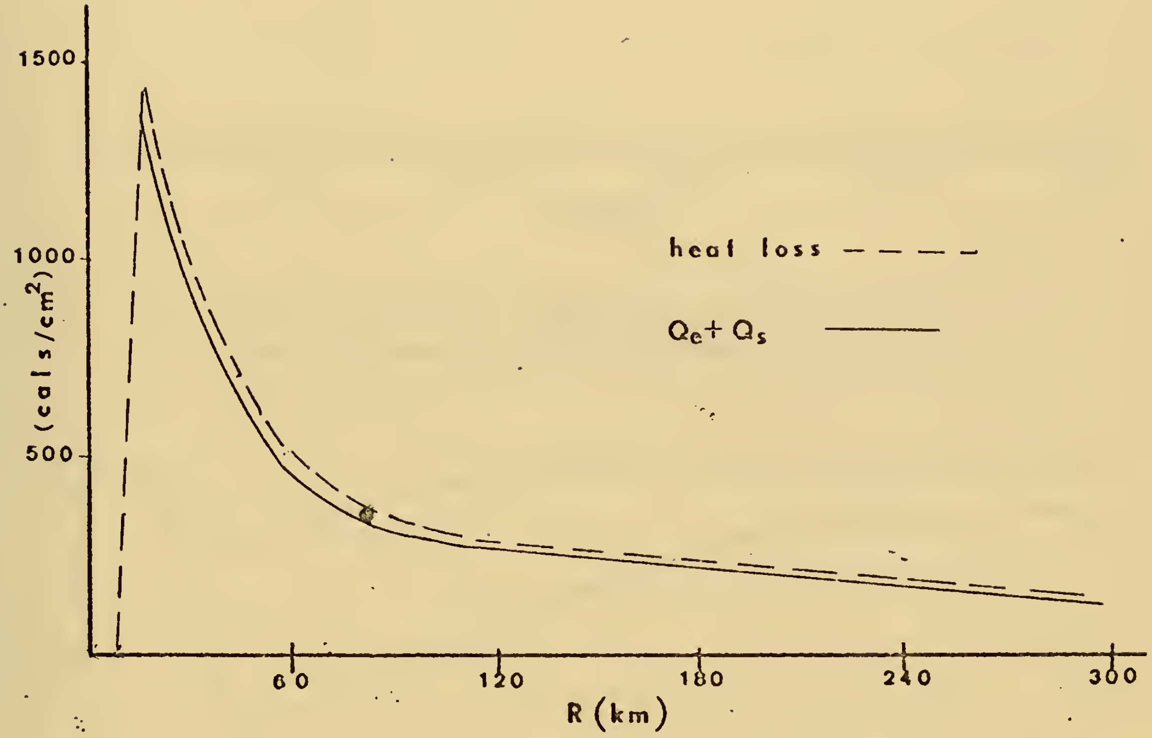

Figure 7. Predicted 18-hour radial profiles of ocean heat loss and accumulated $(Q_E+Q_S)$ from boundary layer model.

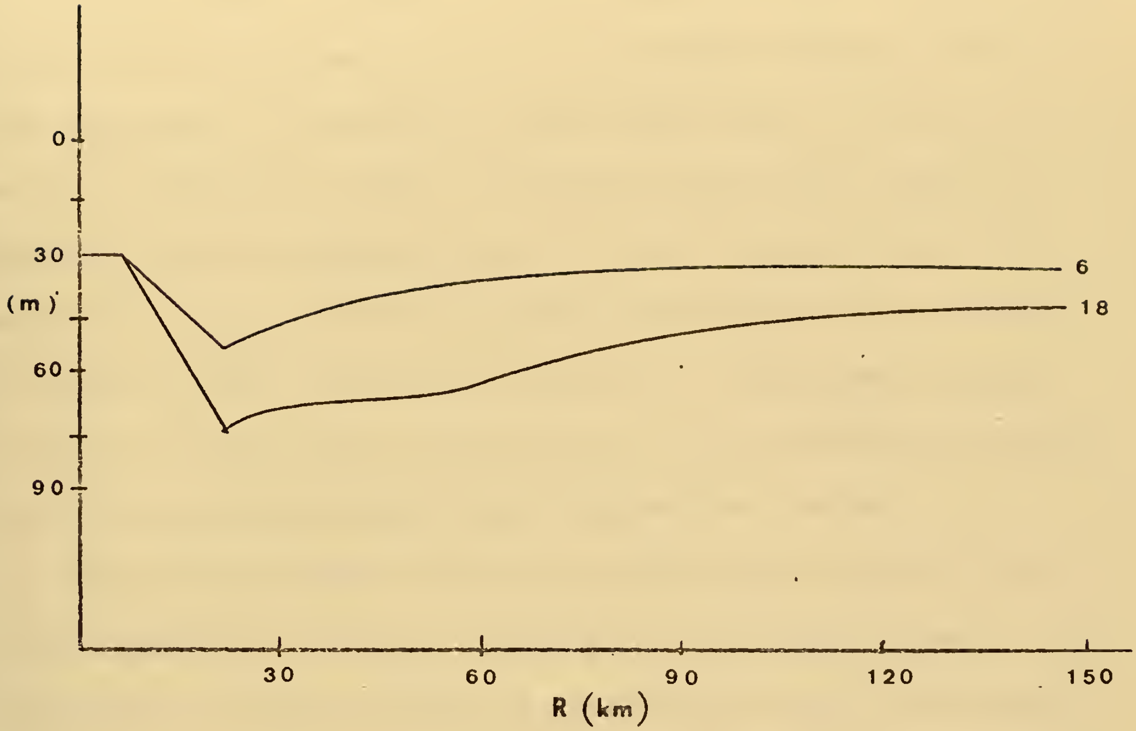

Figure 8. Radial profiles of mixed-layer depth at 6 and 18 hours for entrainment mixing.

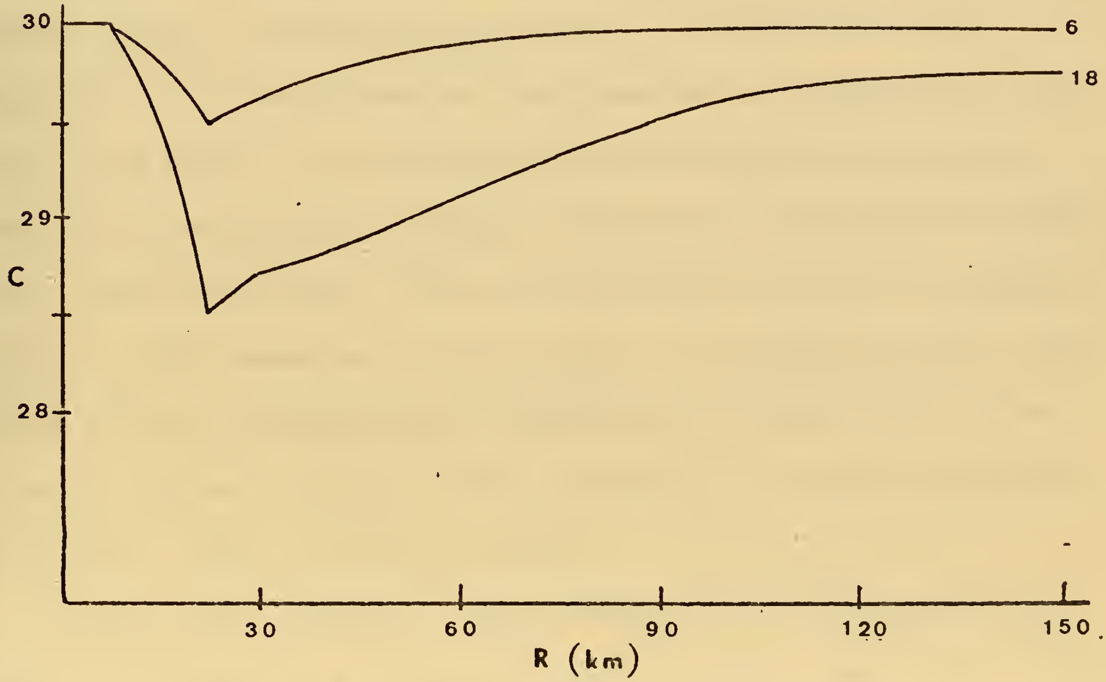

Figure 9. Same as Figure 8 except mixed-layer temperature.

the forcing which produced entrainment mixing through surface turbulent generation (G). Maximum cooling (0.5C) and deepening (23 meters) at six hours and 1.5C and 45 meters at 18 hours again occurred beneath the region of maximum kinetic energy input (28) as expected from (25) and (26). The increased cooling and deepening with time at larger radial distances was due to the outward migration of the hurricane eye wall ($r_i$) in response to colder sea-surface temperatures near the vortex center.

Since entrainment mixing produced only vertical heat redistribution, the heat content of the ocean beneath the atmospheric vortex should be conserved except for numerical errors. Figure (10) depicts the radial distribution of oceanic heat loss at 18 hours for the entrainment-only experiment. The area averaged heat loss for the solution domain (Table II) was 137 cals/cm$^2$. Considering the sensitivity of heat content to changes in temperature and depth and since the depth and temperature solutions were computed numerically, and are subject to truncation errors, the values in Figure (10) are considered within acceptable limits. For example, in the region of maximum mixed-layer depth (75m), a temperature difference of 0.1C will give a heat contant change of 750 cals/cm$^2$. The maximum error in Figure (10) is 800 cals/cm$^2$.

Figure (11) depicts ocean temperature profiles at 6, 12, and 18 hours as computed in the model. Note the strong

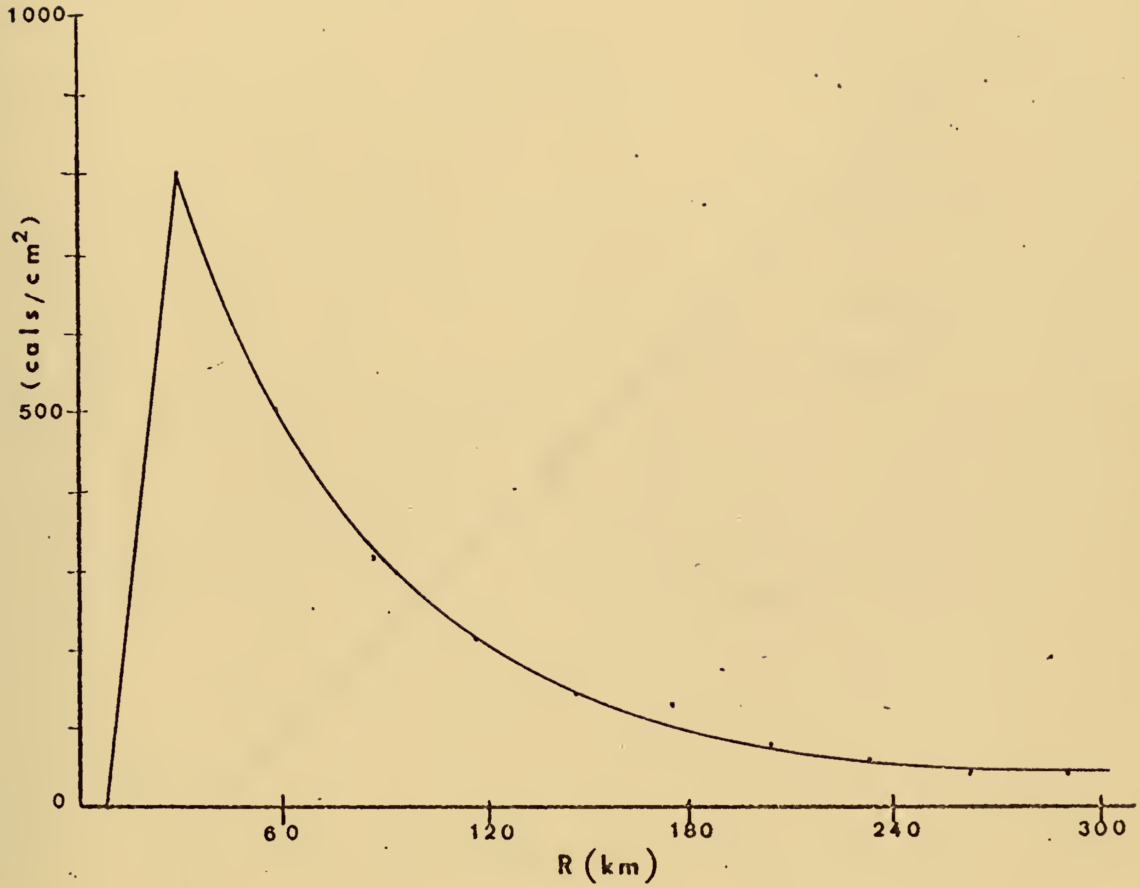

Figure 10. Predicted 18-hour radial profile of ocean heat loss for entrainment mixing.

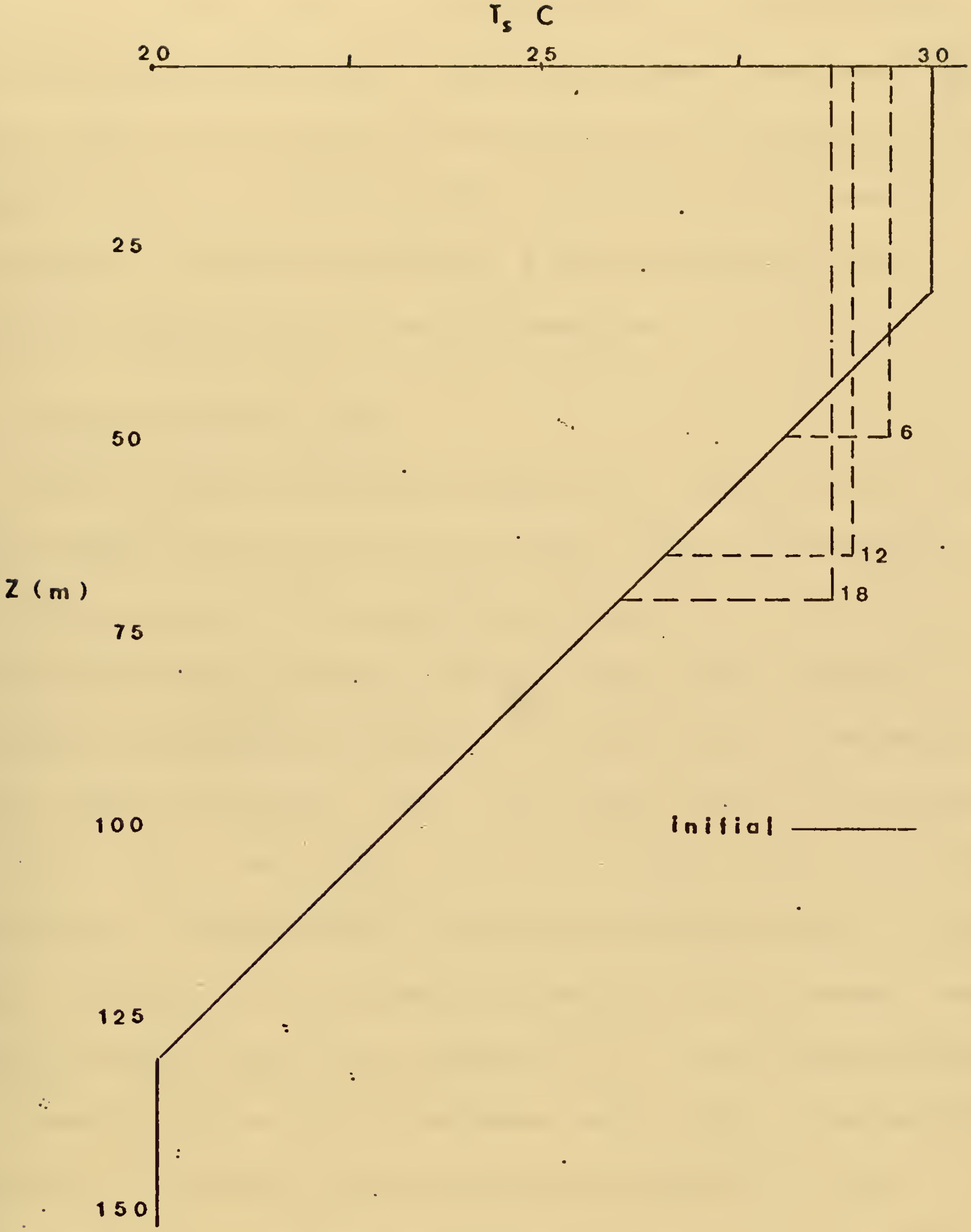

Figure 11. Predicted 6-, 12-, and 18-hour vertical temperature profiles at 30 km for entrainment mixing.

gradient which develops below the mixed layer. As mentioned in a previous section, the temperature difference ($T_s - T_h$) is the primary retarding force which balances the atmospheric forcing. The below-layer gradient ($\frac{\partial T}{\partial Z}$) is an important factor in determining the depth at which this balance will occur. For a given energy input (G), one expects deeper mixing for a weak gradient and shallower mixing for a strong gradient.

## C. ADVECTION-ONLY CASE

For the advection-only case (G=0, and $Q_E + Q_S = 0$), mixed-layer depth and temperature changes were determined by the advection terms in the predictive equations [(25) and (26)]. The partitioning process (29) was not used, hence, all available atmospheric stress ($\tau_a$) was used to produce a radial mass transport (32) and a mean radial wind-driven current (33). The rapid increase in $\bar{u}_r$ (Figure 12) from the vortex center to the radius of maximum wind ($r_i$) produced a region of horizontal divergence and, hence, enormously strong upwelling (Figure 13). Just beyond radius $r_i$ a small region of convergence and, hence, downwelling occurred. However, the gradual decrease in $\bar{u}_r$ was balanced by the increased radius to maintain a fairly constant total mass transport. Consequently, areas of significant downwelling were not evident within the solution domain (300 km).

The effects of strong upwelling were quite evident in the mixed-layer depth and temperature profiles (Figures

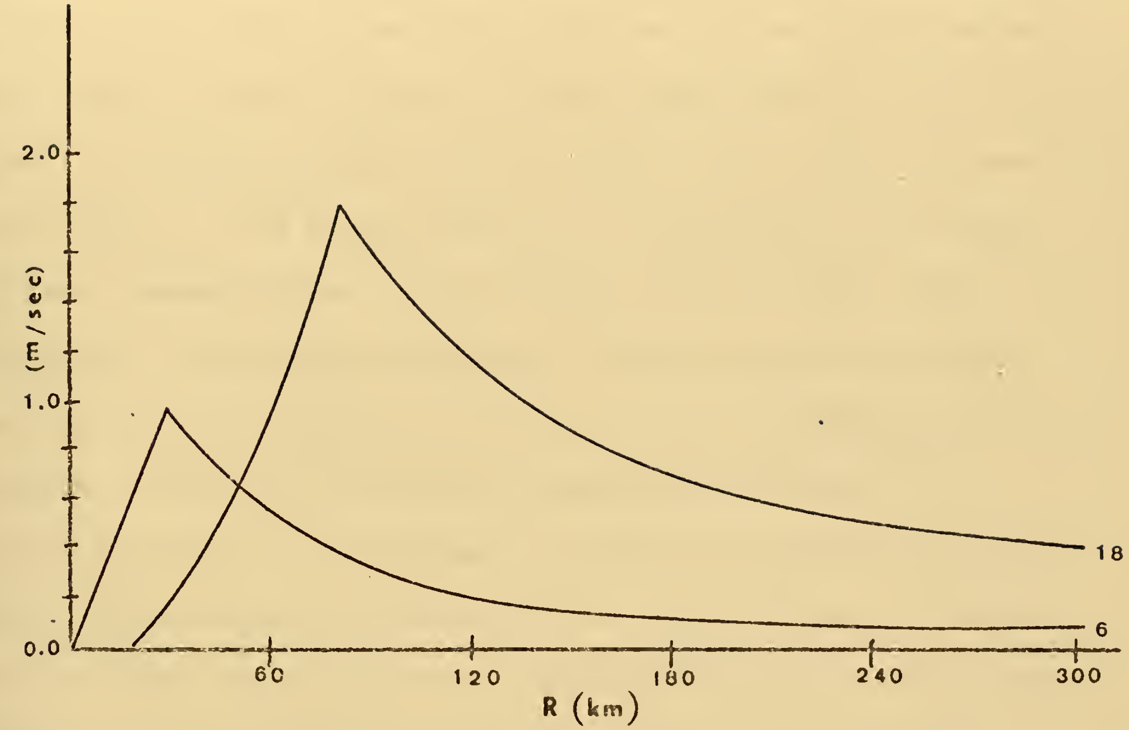

Figure 12. 6- and 18-hour radial profiles of ocean radial velocity for advection-only (no partitioning).

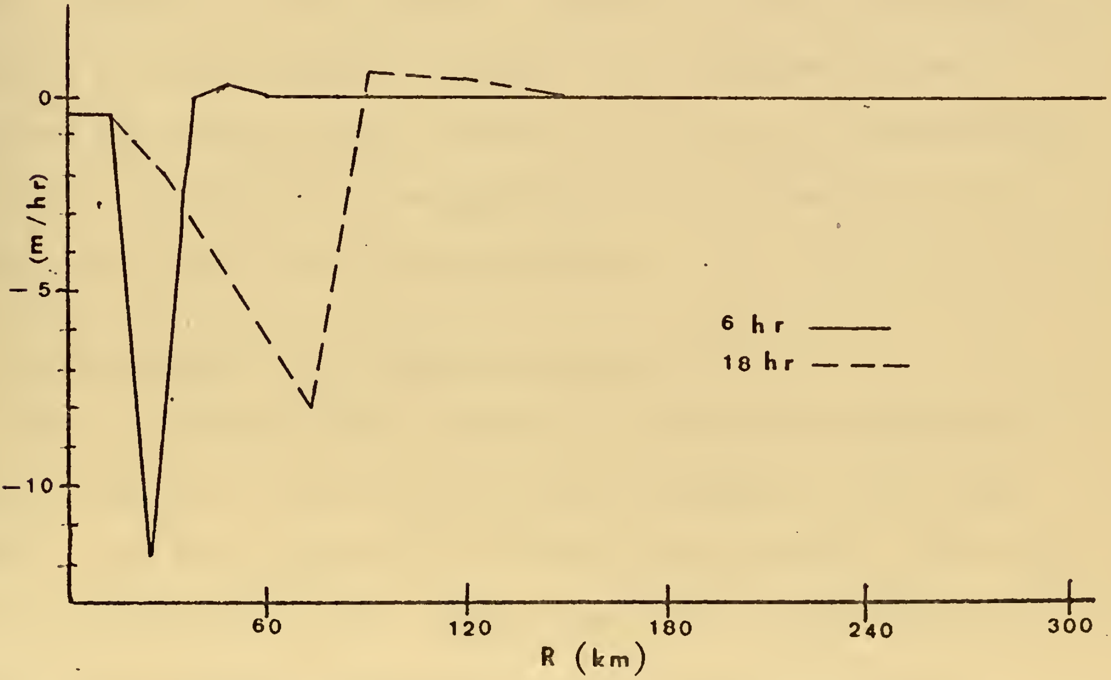

Figure 13. Same as Figure 12 except ocean vertical velocity.

14 and 15). Within six hours the mixed layer, near the vortex center, was eliminated and the sea-surface temperature decreased until the cold deep ocean water (20C) was upwelled to the surface. At 18 hours the radius of maximum wind ($r_i$) had moved outward in response to cold sea-surface temperatures at the vortex center (Figure 16). The region of maximum upwelling likewise moved outward, leaving a broad region of 20C sea-surface temperatures between 15 and 45 km and zero mixed-layer depth to a radius of 95 km. The dramatic effects of advection were also evidenced by significant ocean heat content changes (Figure 17). The positive values correspond to heat loss regions and the negative values to heat gain regions. Vertical and radial velocities produced a redistribution of heat by changing the ocean temperature profile (Figure 18). Because of the ocean's response to the atmospheric stress profile, radial currents ($\bar{u}_r$) transported heat across the model's open boundary at 300 km. Consequently, there's a significant averaged heat loss (Table II) in the ocean model for this experiment.

## D. ENTRAINMENT AND CONVECTIVE MIXING

This experiment was similar to the entrainment-only run except heat flux ($Q_E + Q_S$) was included in (25) and (26). For the initial run, stress partitioning (29) was utilized with $C = 10^4$. Radial profiles of mixed-layer depth (Figure 19) and temperature (Figure 20) closely

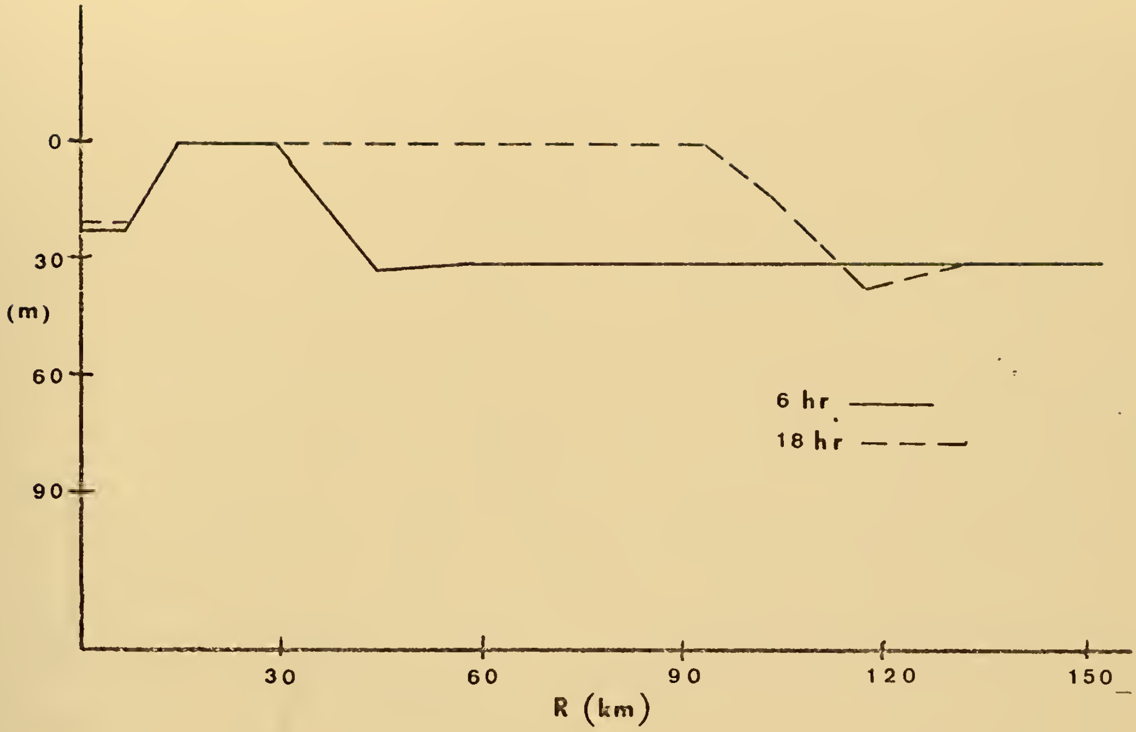

Figure 14. Same as Figure 12 except mixed-layer depth.

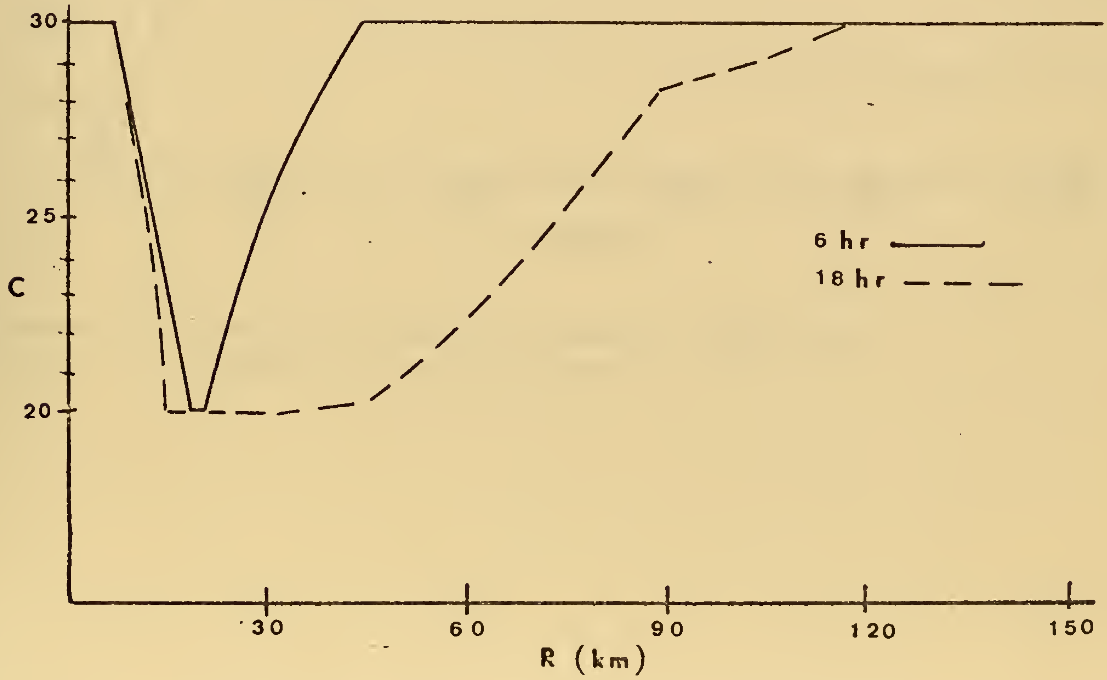

Figure 15. Same as Figure 12 except mixed-layer temperature.

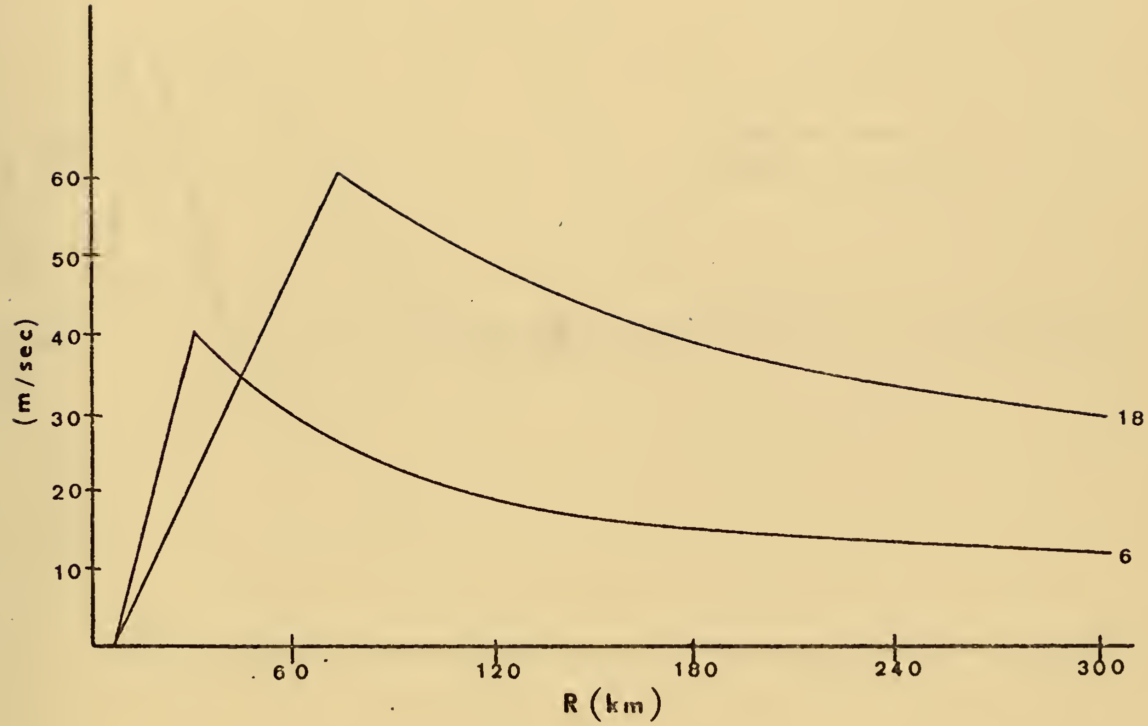

Figure 16. Same as Figure 12 except tangential component of the wind.

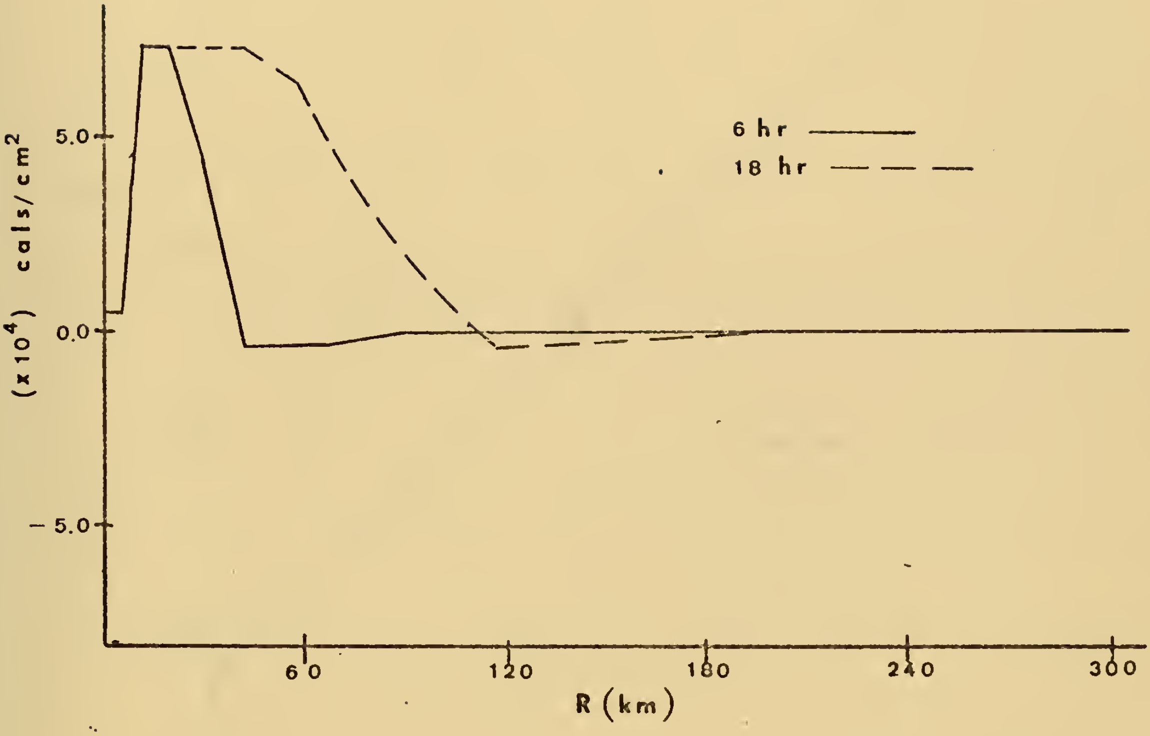

Figure 17. Same as Figure 12 except ocean heat loss.

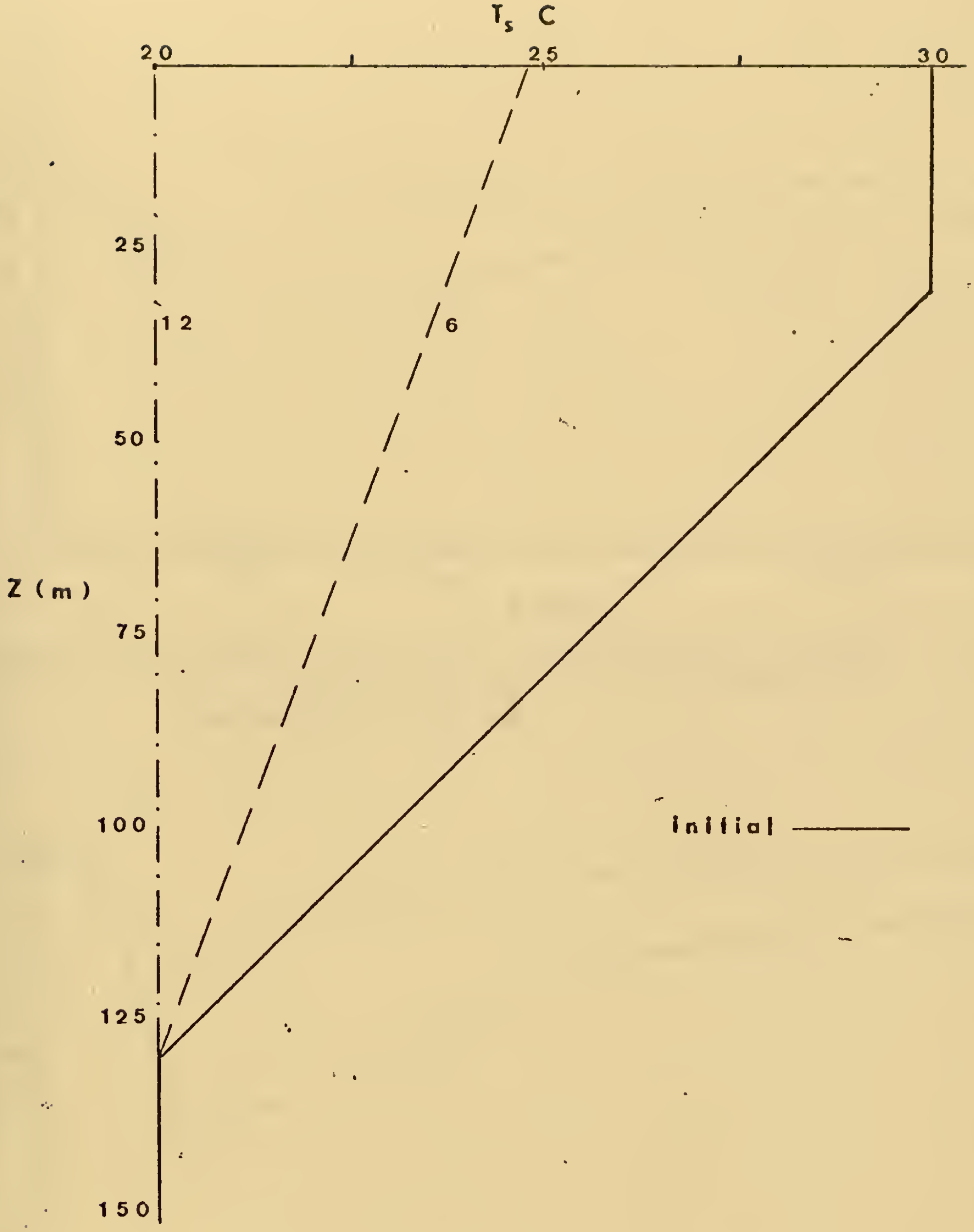

Figure 18. Predicted 6- and 12-hour vertical temperature profiles at 30 km for advection only.

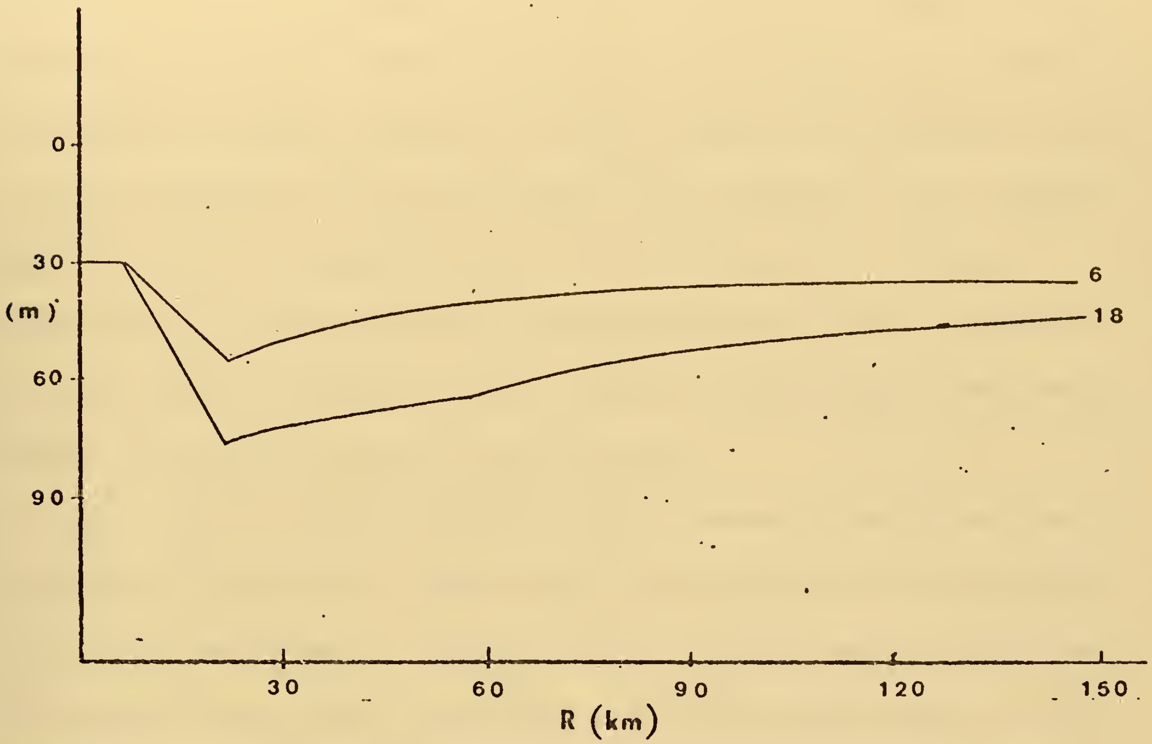

Figure 19. Radial profiles for mixed-layer depth at 6 and 18 hours for entrainment and convective mixing.

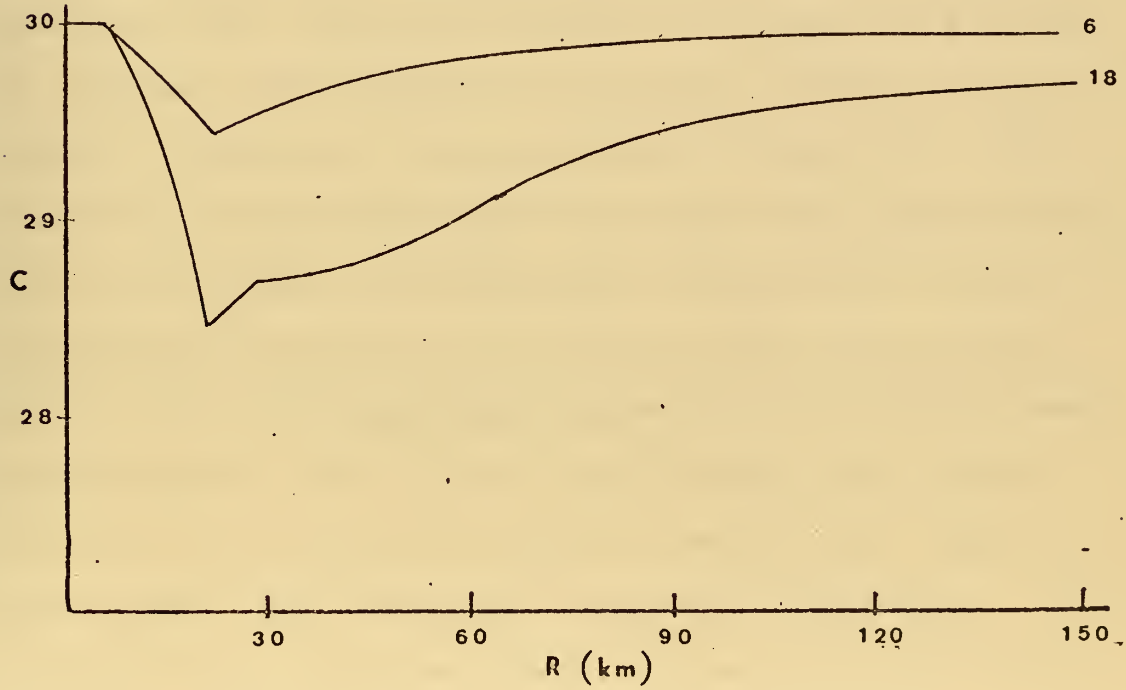

Figure 20. Same as Figure 19 except mixed-layer temperature.

resemble the corresponding profiles for entrainment-only (Figures 8 and 9). The inclusion of the heat flux term produced a slight increase in the amount of deepening and cooling compared to entrainment-only; however, the amount was less than 2 meters and 0.5C at 18 hours. One may conclude that entrainment mixing dominates when compared to convective mixing for the initial conditions and atmospheric forcing utilized in the model.

For this run the oceanic heat content should not be conserved because of the latent and sensible heat exchange with the atmosphere. Figure (21) depicts radial profiles of oceanic heat loss, calculated in the ocean model, and heat extraction (H) from the boundary-layer model. The difference between the profiles represents the loss attributed to inaccuracies in the numerical solution of (25), (26), and (27), and unfortunately is as large as H itself. The vertical ocean temperature profiles (Figure 22) were similar to those for entrainment-only (Figure 11). For comparison, Figures (23) and (24) show radial profiles of mixed-layer depth and temperature, respectively, for an entrainment-convection run in which stress partitioning was not used. All available stress ($\tau_a$) from the boundary-layer model was used in the kinetic energy term (G) of (25) and (26) to produce changes in mixed-layer depth and temperature. The increased atmospheric forcing was evidenced by an increased maximum mixed-layer depth (12 m

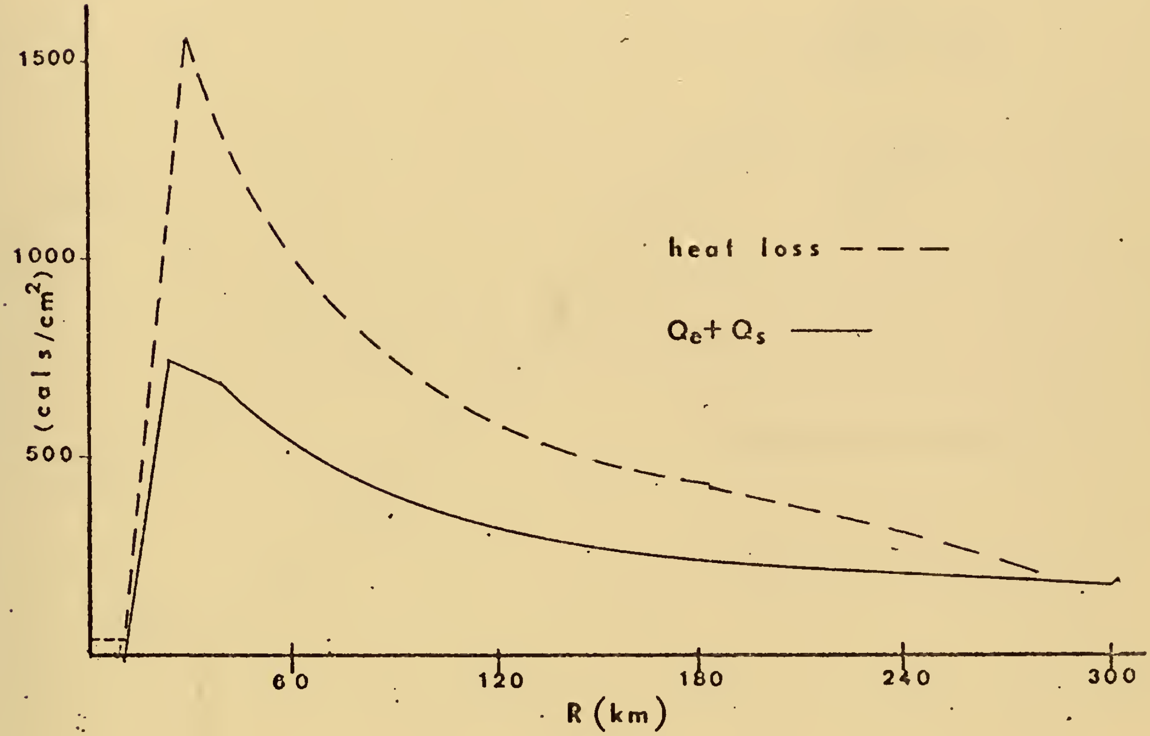

Figure 21. Predicted 18-hour radial profiles of ocean heat loss and accumulated $(Q_E + Q_S)$ from boundary-layer model.

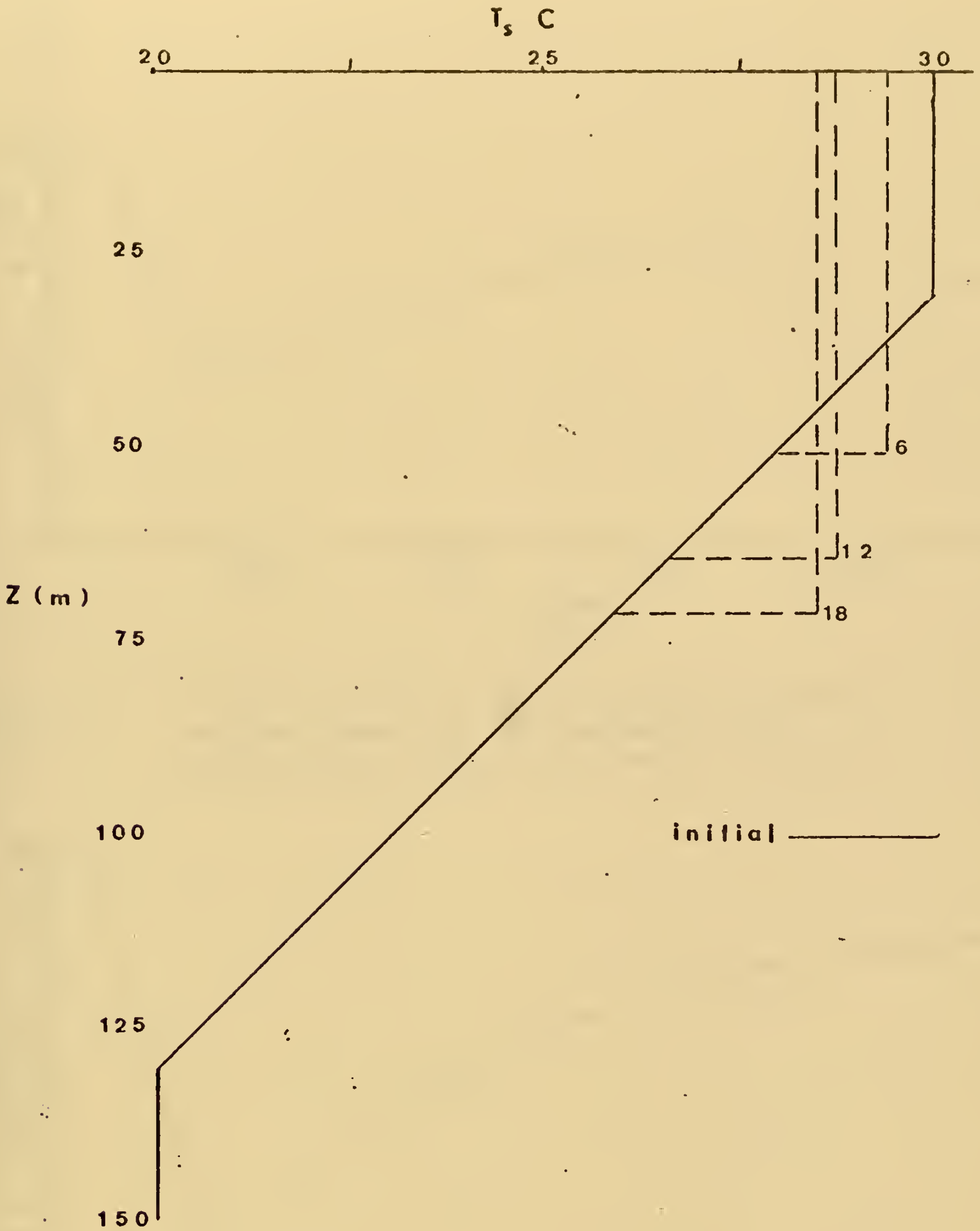

Figure 22. Same as Figure 11 except for entrainment and convective mixing.

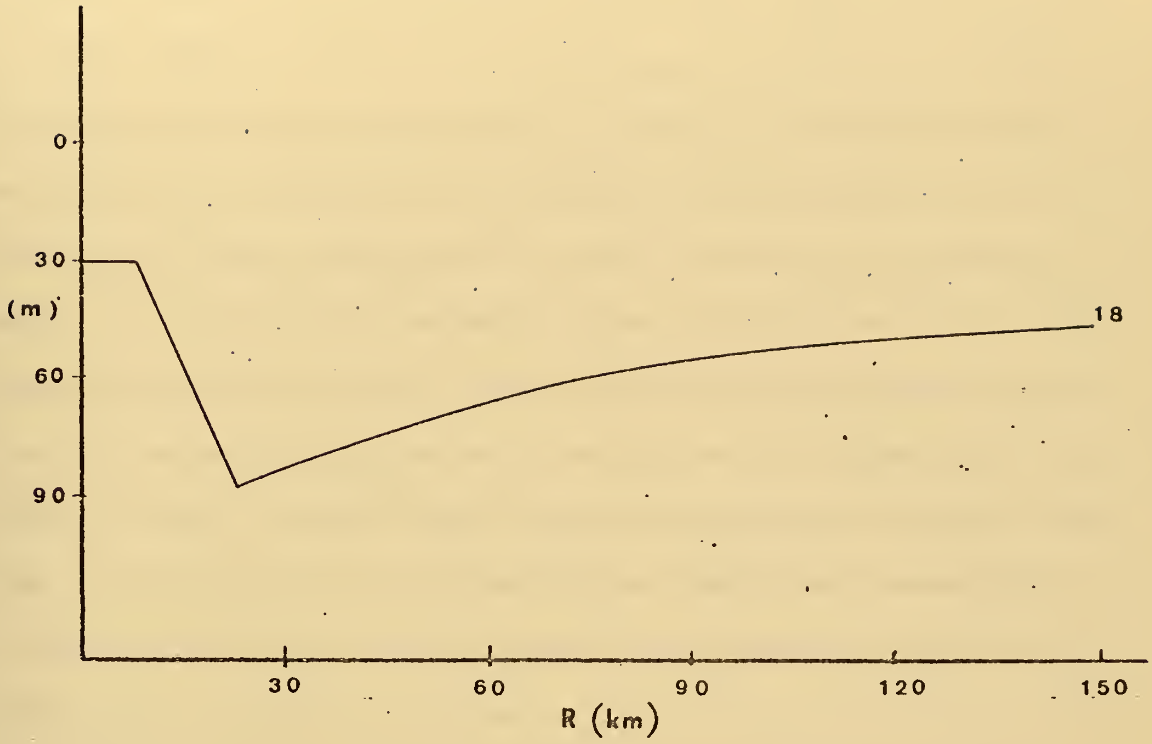

Figure 23. Radial profile of mixed-layer depth at 18 hours for entrainment and convective mixing (no partitioning).

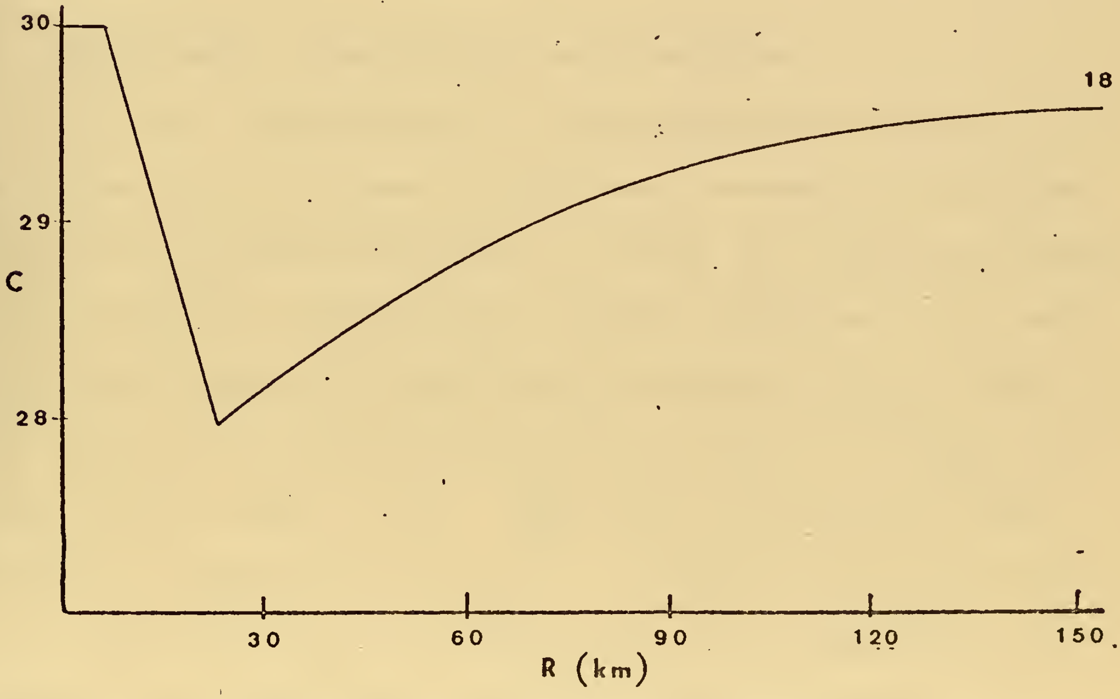

Figure 24. Same as Figure 23 except mixed-layer temperature.

deeper) and a lower minimum mixed-layer temperature (.5C colder) than for the partitioned run. In both of these entrainment-convection runs, as well as the entrainment-only run, the amount of sea-surface cooling near the vortex center was sufficient to cause the radius of maximum wind ($r_i$) to migrate outward. The intensification of the atmospheric forcing at larger radii produced a corresponding increased deepening and cooling of the mixed layer at larger radii. Since there was no upwelling in these runs, the radial profiles of mixed-layer depth and temperature were not modified, and the radius of maximum cooling and deepening remained at 20 km.

In the next set of experiments advection will be included and the effect of variations in the partitioning constant (C) will be examined.

## E. ENTRAINMENT, CONVECTION, AND ADVECTION

This run incorporated all the mechanisms believed to be of importance in cooling the ocean beneath a hurricane. The total available atmospheric stress ($\tau_a$) was partitioned (29) into that which produced surface turbulence ($\tau_o$) and that which generated wind-driven currents ($\tau_a - \tau_o$). For the initial run the partitioning constant (C) in Equation (29) was set equal to $10^4$. This gave a stress vs. depth profile as depicted in Table I. In addition to the kinetic energy and flux terms, advective terms were included in the solution for mixed-layer depth (26) and temperature (25).

The radial advection velocity ($\bar{u}_r$) was specified according to (33) and areas of vertical velocities ($\bar{w}$) were calculated from (34). Radial profiles of $\bar{u}_r$ (Figure 25) and $\bar{w}$ (Figure 26) were similar in nature to those for advection only (Figures 12 and 13). However, since stress partitioning was not used for the advection-only experiment, the magnitudes of $\bar{u}_r$ and $\bar{w}$ were smaller in the current experiment.

As in previous runs, the hurricane eye wall moved outward in response to cold sea-surface temperatures near the vortex center (Figure 16). The upwelling region (Figure 26) likewise moved outward in response to the movement of maximum surface stress. The changes in mixed-layer depth and temperature produced by entrainment and convective mixing (Figures 19 and 20) were significantly modified by the outward migration of the upwelled region. For the entrainment-convection mixing case the region of maximum mixed-layer deepening was coincident with the region of maximum cooling. However, with the addition of advection, the maximum deepening (Figure 27) occurred at radii just outside the radius of maximum wind ($r_i$), where upwelling was weak and the atmospheric forcing (G and $Q_E + Q_S$) was fairly large. At smaller radii the upwelling dominated the effect of mixing, leaving very shallow mixed-layer depths. The region of maximum ocean cooling (Figure 28), which remained in the vicinity of 15 km, represented an interaction between mixing and advection. By decreasing the layer thickness, upwelling

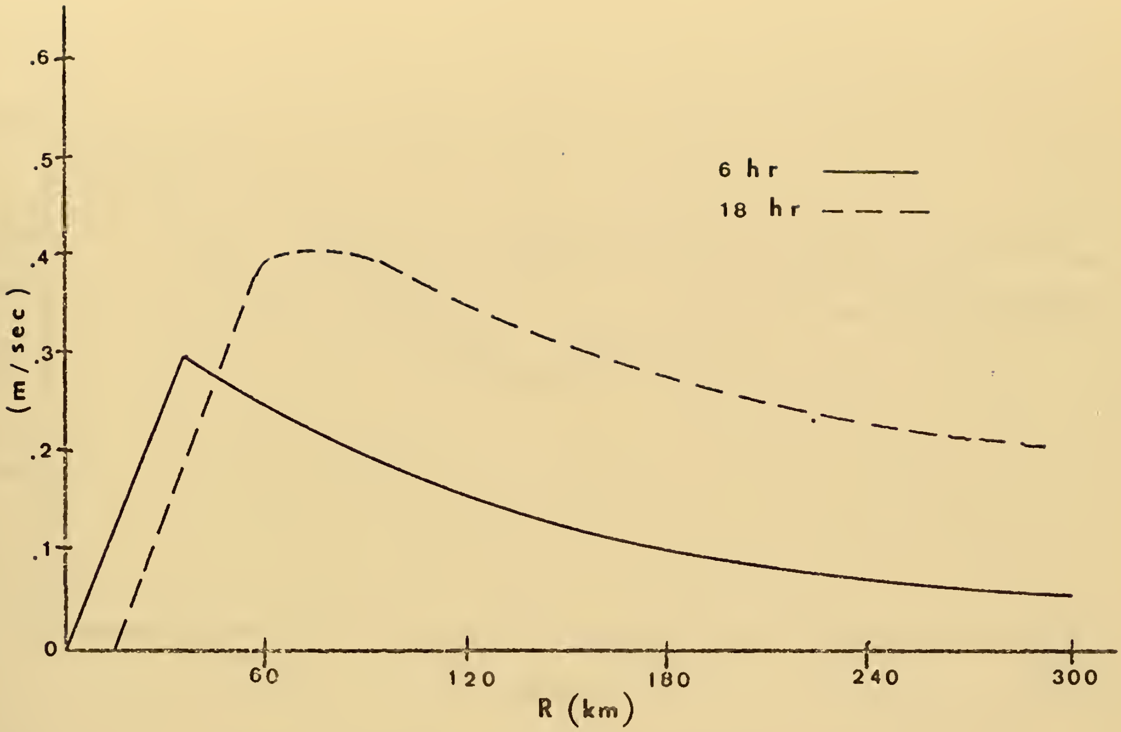

Figure 25. 6- and 18-hour radial profiles of ocean radial velocity for entrainment, convection, and advection (partitioning, $C=10^4$).

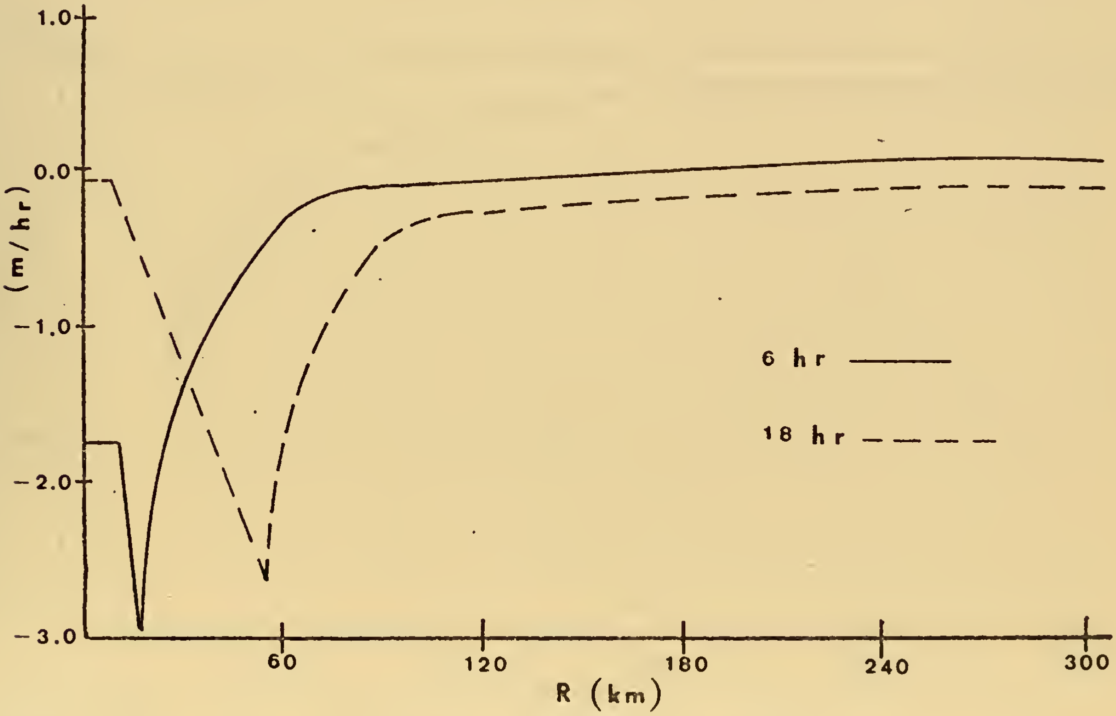

Figure 26. Same as Figure 25 except ocean vertical velocity.

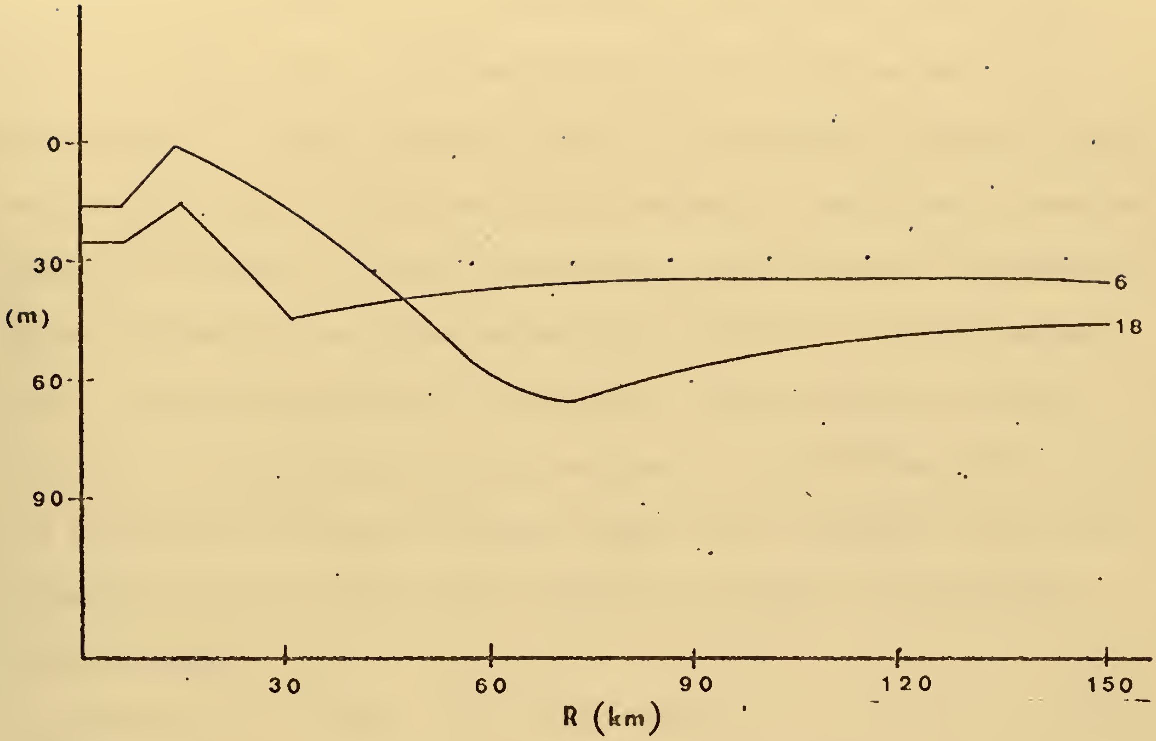

Figure 27. Same as Figure 25 except mixed-layer depth.

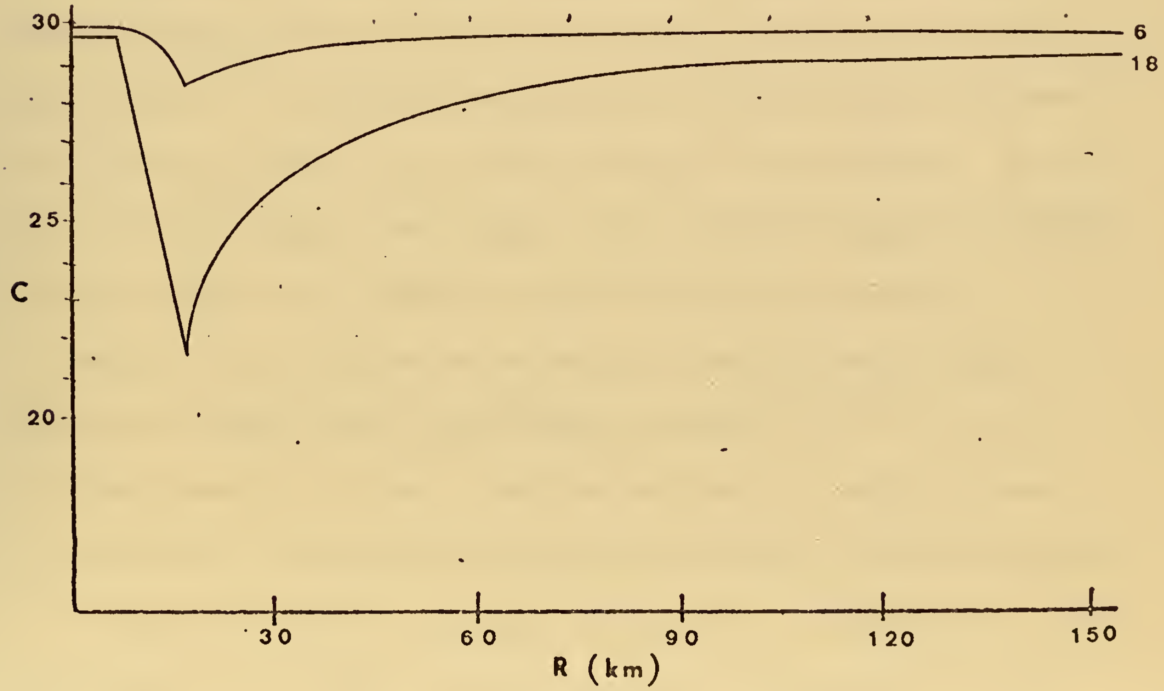

Figure 28. Same as Figure 25 except mixed-layer temperature.

enhanced the effects of atmospheric forcing on the mixed-layer cooling (25). Stress partitioning increased the percentage of total stress used in the kinetic energy term (G) as the mixed-layer depth decreased. There was a corresponding decrease in the stress used for currents (upwelling) which tended to keep the mixed-layer depth from becoming zero. Since ultimately it was the value of the constant (C) which determined whether mixing or upwelling would have the greatest influence on the mixed-layer depth, the entire formulation of stress partitioning deserves considerable future study.

Significant ocean heat loss (Figure 29) occurred inside 30 km where upwelling had the greatest effect on the vertical temperature profile (Figure 30). At larger radii, where entrainment and convection dominated, ocean heat content changes reflected the heat extraction (H) by the boundary-layer model. The area averaged heat loss (Table II) for the solution domain was 2300 $\text{cals/cm}^2$ at 18 hours. As in the advection-only case, this loss reflects the transport of heat across the model's open boundary at 300 km.

To test the influence of stress partitioning (29), a second experiment was run using a value of $C = 5 \times 10^3$. With this smaller value, the percentage of total stress ($\tau_a$) used for entrainment mixing was smaller and decreased more rapidly with mixed-layer depth and, consequently, the percentage of stress used for current generation ($\tau_a - \tau_o$)

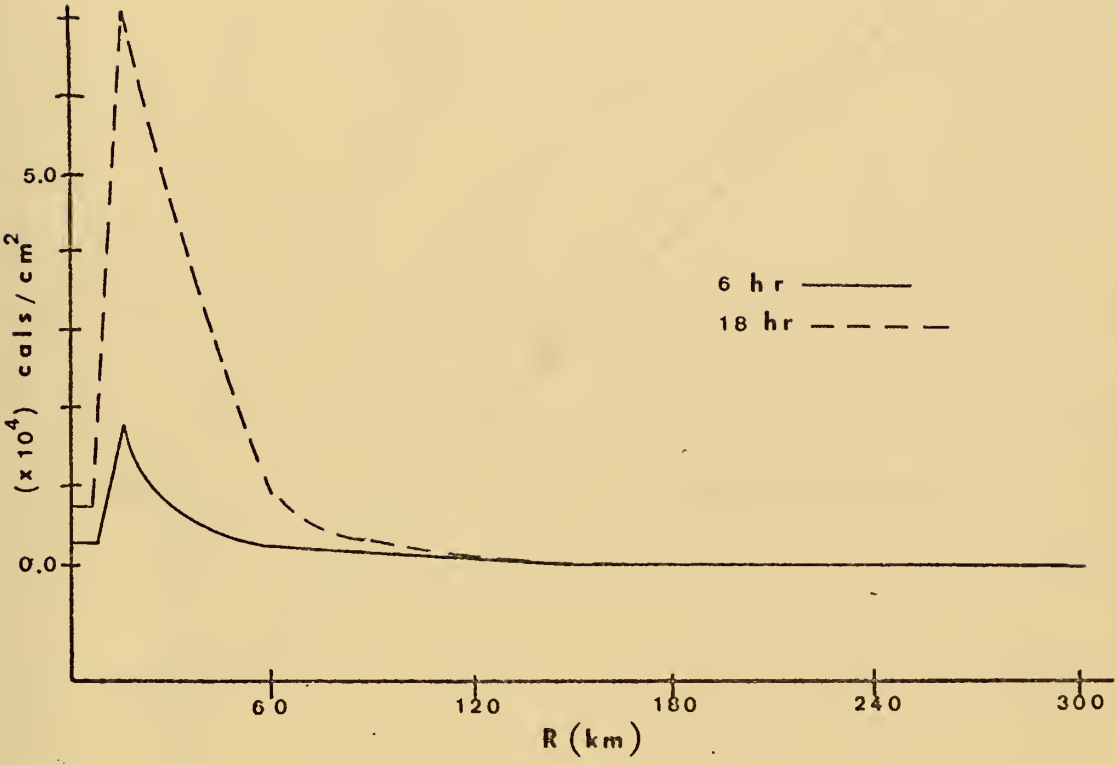

Figure 29. Predicted 6- and 18-hour radial profiles of ocean heat loss for entrainment, convection, and advection.

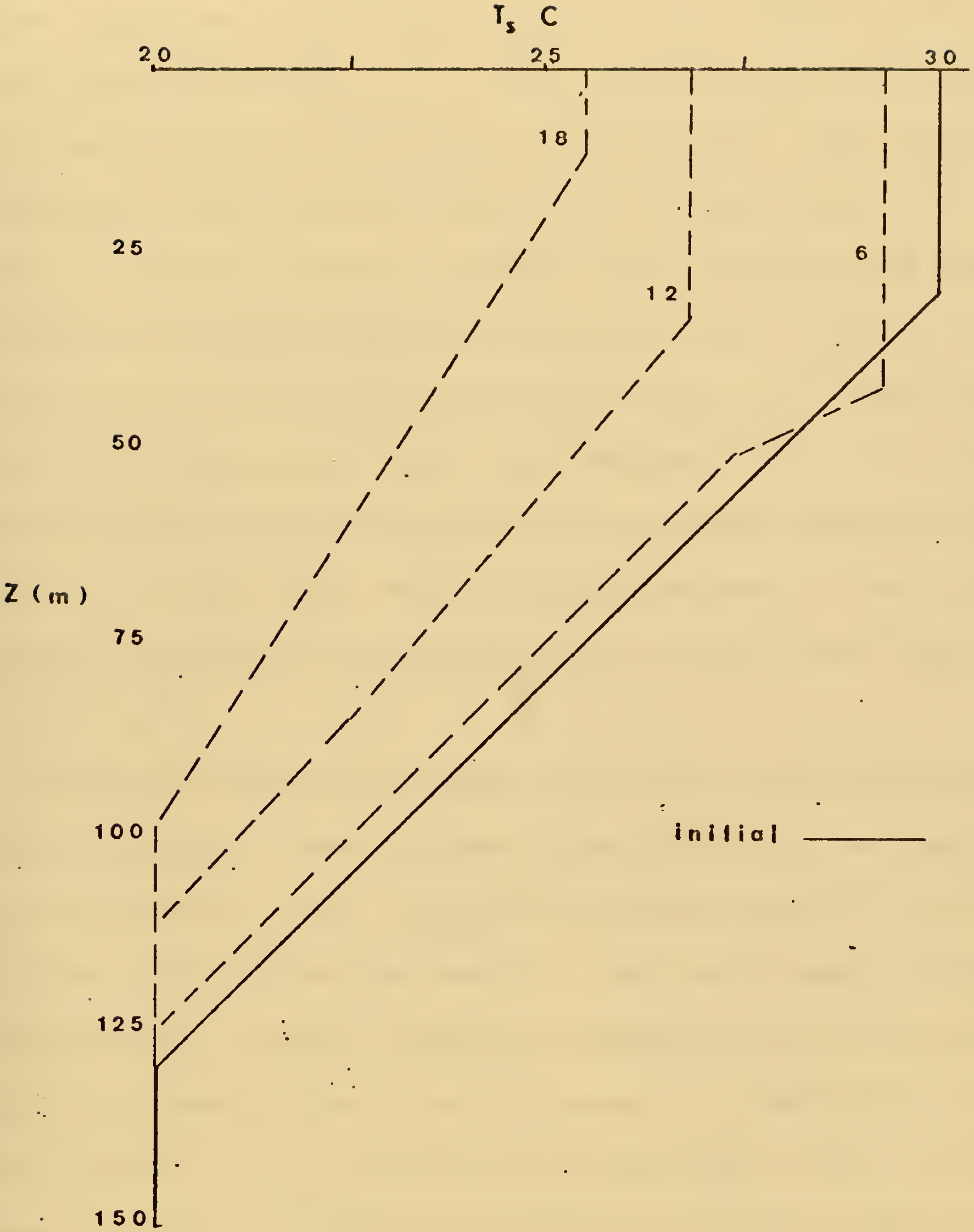

Figure 30. Same as Figure 11 except entrainment, convection, and advection.

was larger and increased more rapidly with mixed-layer depth (Table I). Comparing radial profiles of mixed-layer depth and temperature for $C = 10^4$ [Figures (27) and (28)] with those for $C = 5 \times 10^3$ [Figures (31) and (32)], it is apparent that advection by horizontal and vertical velocities had a greater influence in the latter case. [Note similarity between Figures (31) and (32) and those for advection only Figures (14) and (15)]. For $C = 5 \times 10^3$ upwelling has eliminated the mixed layer in a small region near the vortex center and the combined effects of upwelling and mixing have cooled the sea-surface temperature to 20C. At larger radii where mixing dominates, there was greater deepening and cooling with $C = 10^4$ than with $C = 5 \times 10^3$.

Table II summarizes some significant atmospheric and ocean variables. The air-sea interaction was evident in all cases where there was pronounced cooling of the ocean surface near the vortex center. The lower sea-surface temperatures reduced the air-sea temperature difference, hence the heat fluxes from the ocean to the boundary layer were reduced. The tendency for the model's eye wall to seek a region of maximum equivalent potential temperature ($\theta_e$) caused the radius of maximum wind ($r_i$) to move outward as the inner surface was cooled (Figure 16). This outward migration maintained a sufficient equivalent potential temperature difference ($\theta_{e_i} - \theta_{e_o}$) and, consequently, the

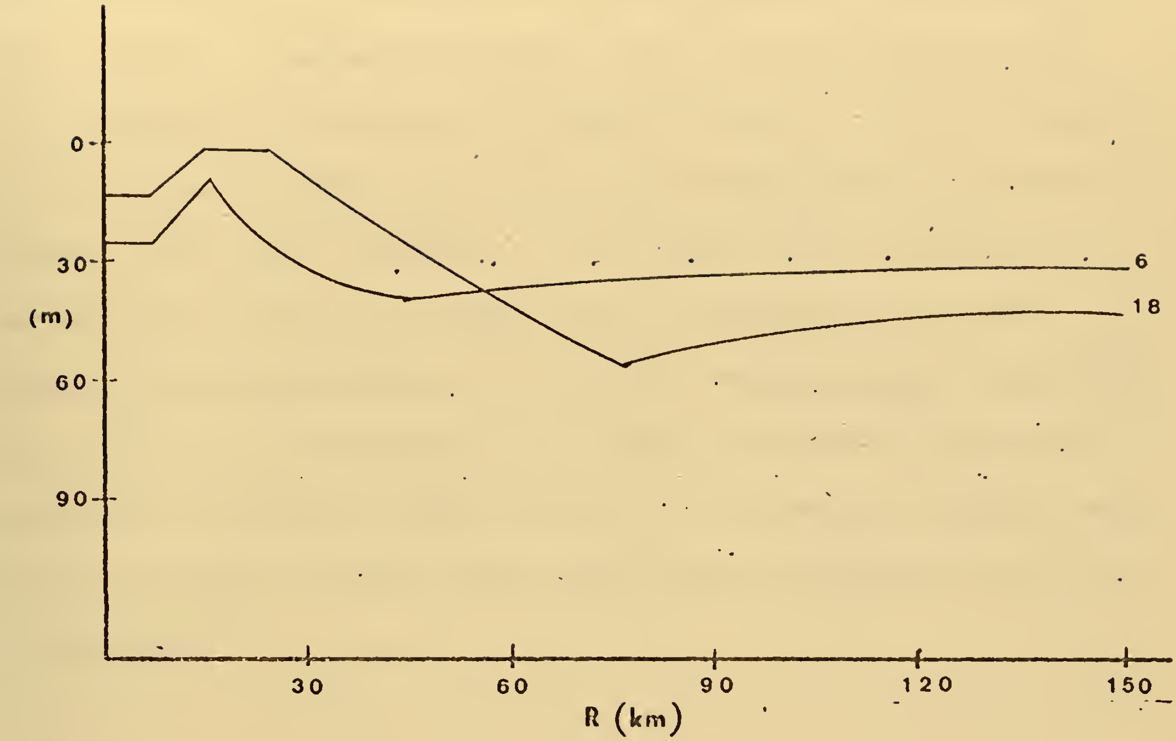

Figure 31. Same as Figure 27 except $C=5x10^3$.

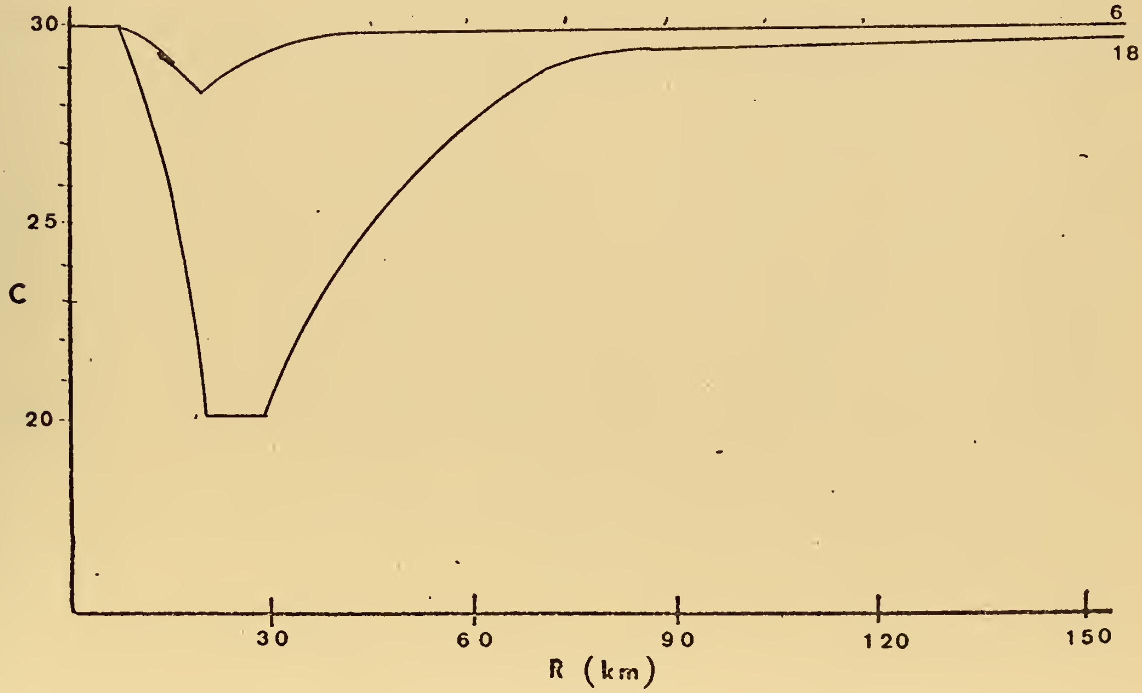

Figure 32. Same as Figure 28 except $C=5x10^3$.

maximum wind ($v_{\theta_i}$) remained fairly constant. Because of the $v_\theta r^{1/2}$ = constant profile, the outward migration of $r_i$ produced an unrealistic intensification of the circulation at large radii. This in turn maintained a constant total ocean mass transport with radius which resulted in significant amounts of heat being transported out the model's 300 km boundary to a region where downwelling would presumably have occurred. In order to properly model the movement of the eye wall the $v_\theta r^{1/2}$ = constant profile must be modified to prevent this unrealistic intensification at large radii.

TABLE II

Significant atmospheric and oceanic variables for different experiments at 18 hours.

| | max $h_o$ (m) | min $T_s$ (C) | $v_{\theta_i}$ (m/sec) | $r_i$ (km) | Area Average ocean heat loss (cals/cm$^2$) | Area Average H (cals/cm$^2$) |
|---|---|---|---|---|---|---|
| Convection | 35 | 29.5 | 60 | 21 | 252 | 240 |
| Entrainment | 75 | 28.5 | 58 | 54 | 137 | --- |
| Advection (No Partitioning) | 32 | 20.0 | 60 | 78 | 5300 | --- |
| Entrainment and Convection | | | | | | |
| Partitioning | 76 | 28.4 | 58 | 57 | 437 | 262 |
| No partitioning | 88 | 27.9 | 56 | 51 | 578 | 214 |
| Entrainment, Convection and Advection | | | | | | |
| $C = 10^4$ | 66 | 21.7 | 59 | 72 | 2300 | 288 |
| $C = 5 \times 10^3$ | 56 | 20.0 | 59 | 66 | 1854 | 260 |

# IV. SUMMARY AND CONCLUSIONS

The results of this study indicate the feasibility of coupling an ocean model to an atmospheric vortex model to simulate time-dependent air-sea interaction. Since the model was stationary, and the effects of large-scale ocean current, turbulent-scale energy dissipation, radiation, and internal waves were not included, the magnitude of the ocean thermal changes may not be representative. However, the relative changes for the various cooling mechanisms (convective mixing, entrainment mixing, and advection) were apparent.

First, convective mixing had insignificant effects on an ocean thermal structure initialized with 30 meter mixed-layer depth, 30C mixed-layer temperature, and below-layer gradient of 10C/100m. Convective cooling would have been more pronounced for shallower layer depths and stronger below-layer gradients; however, these were not tested in the model.

Second, entrainment (wind) mixing produced fairly substantial mixed-layer deepening and cooling in the region of maximum wind stress. The radius of maximum wind responded to the colder sea-surface temperatures by migrating outward. The effect of entrainment mixing, likewise, moved outward producing deeper layer depths and colder sea-surface temperatures at larger radii. The depth and

temperature changes due to entrainment and convection were comparable to those for entrainment only indicating entrainment to be the dominate process.

Third, the effects of the wind-driven circulation, when acting alone, produced the most pronounced changes in mixed-layer depth and temperature. Upwelling inside the radius of maximum wind displaced the relatively warm mixed-layer water by cold deep-ocean water advected from below. The warm surface-layer water was advected outward by radial currents. Since no significant downwelling occurred within the solution domain, heat was lost through the model's outer boundary.

In reality the various mechanisms studied do not act separately but rather interact in some complex fashion to produce the thermal changes which observations have shown. It appeared to be a question between entrainment mixing and advection as to which has the dominate role in cooling sea-surface temperatures beneath a hurricane. Advection definitely produced significant cooling inside the radius of maximum wind but to think of a wind-driven circulation with no surface turbulence seems unrealistic. It appeared that the interaction of the two processes, with a budgeting of the total atmospheric stress between turbulence generation and current generation, was the dominate mechanism for sea-surface cooling.

# BIBLIOGRAPHY

1. Blackadar, A. K., 1965: A simplified two-layer model of the baroclinic neutral atmosphere boundary layer. Air Force Cambridge Research Laboratories Report 65-531, pp. 49-65.

2. Cardone, V. J., 1969: Specification of the wind distribution in the marine boundary layer for wave forecasting. New York University, School of Engineering and Science, Scientific Report GSL-TR69-1, University Heights, New York.

3. Corgnati, L. B., 1971: Experiments with a simple hurricane-interacting ocean model, M.S. Thesis, Naval Postgraduate School, Monterey.

4. Denman, K. L., 1973: A time-dependent model of the upper ocean. Journal of Physical Oceanography, 3, 173-184.

5. Elsberry, R. L., N. A. S. Pearson, and L. B. Corgnati, 1973: Experiments with a simple hurricane-ocean interaction model. Submitted for publication.

6. Fisher, E. L., 1958: Hurricanes and the sea-surface temperature field. J. Meteor., 15, 328-333.

7. Jordan, C. L., 1964: On the influence of tropical cyclones on the sea-surface temperature field. Proc. Symp. Trop. Meteor., New Zealand Meteor. Service, Wellington, 614-622.

8. Kraus, E. B., and J. S. Turner, 1967: A one-dimensional model of the seasonal thermocline. Tellus, 19, 88-106.

9. Leipper, D. F., 1967: Observed ocean conditions and hurricane Hilda, 1964. J. Atmos. Sci., 24, 182-196.

10. Pearson, N. A. S., 1972: Further experiments with an hurricane-ocean interaction model, M.S. Thesis, Naval Postgraduate School, Monterey.

11. Riehl, H., 1963: Some relations between wind and thermal structure of steady-state hurricanes. Journal Atmospheric Sciences, 20, 276-287.

12. Shea, D. J. and W. M. Gray, 1972: The structure and dynamics of the hurricanes inner core region. Department of Atmospheric Science, Colorado State University, Atmospheric Science Paper No. 182, Fort Collins, 134.

# INITIAL DISTRIBUTION LIST

| | | No. Copies |
|---|---|---|
| 1. | Defense Documentation Center<br>Cameron Station<br>Alexandria, Virginia 22314 | 2 |
| 2. | Library, Code 0212<br>Naval Postgraduate School<br>Monterey, California 93940 | 2 |
| 3. | Professor R. L. Elsberry, Code 51Es<br>Department of Meteorology<br>Naval Postgraduate School<br>Monterey, California 93940 | 8 |
| 4. | Professor D. F. Leipper, Code 58Lr<br>Department of Oceanography<br>Naval Postgraduate School<br>Monterey, California 93940 | 1 |
| 5. | Lieutenant T. S. Fraim<br>Atkron 42<br>Naval Air Station Oceana<br>Virginia Beach, Virginia 23460 | 3 |
| 6. | Lieutenant Commander N. A. S. Pearson<br>Helicopter Support Squadron Seven<br>Naval Air Station Imperial Beach<br>Imperial Beach, California 92032 | 1 |
| 7. | Naval Weather Service Command<br>Naval Weather Service Command Headquarters<br>Washington Navy Yard<br>Washington, D. C. 20390 | 1 |
| 8. | Department of Meteorology<br>Code 51<br>Naval Postgraduate School<br>Monterey, California 93940 | 2 |
| 9. | Professor R. L. Haney, Code 51Hy<br>Department of Meteorology<br>Naval Postgraduate School<br>Monterey, California 93940 | 1 |
| 10. | Professor R. J. Renard, Code 51Rd<br>Department of Meteorology<br>Naval Postgraduate School<br>Monterey, California 93940 | 1 |

11. Environmental Prediction Research Facility 1
Naval Postgraduate School
Monterey, California 93940

12. Naval Oceanographic Office 1
Library (Code 3330)
Washington, D. C. 20373

| | | |
|---|---|---|
| REPORT DOCUMENTATION PAGE | | READ INSTRUCTIONS<br>BEFORE COMPLETING FORM |
| 1. REPORT NUMBER | 2. GOVT ACCESSION NO. | 3. RECIPIENT'S CATALOG NUMBER |
| 4. TITLE (and Subtitle)<br>Oceanic Thermal Response to a Time-Dependent Hurricane Model | | 5. TYPE OF REPORT & PERIOD COVERED<br>Master's Thesis<br>September 1973 |
| | | 6. PERFORMING ORG. REPORT NUMBER |
| 7. AUTHOR(s)<br>Thomas Stewart Frain | | 8. CONTRACT OR GRANT NUMBER(s) |
| 9. PERFORMING ORGANIZATION NAME AND ADDRESS<br>Naval Postgraduate School<br>Monterey, California 93940 | | 10. PROGRAM ELEMENT, PROJECT, TASK AREA & WORK UNIT NUMBERS |
| 11. CONTROLLING OFFICE NAME AND ADDRESS<br>Naval Postgraduate School<br>Monterey, California 93940 | | 12. REPORT DATE<br>September 1973 |
| | | 13. NUMBER OF PAGES<br>71 |
| 14. MONITORING AGENCY NAME & ADDRESS(if different from Controlling Office)<br>Naval Postgraduate School<br>Monterey, California 93940 | | 15. SECURITY CLASS. (of this report)<br>Unclassified |
| | | 15a. DECLASSIFICATION/DOWNGRADING SCHEDULE |

16. DISTRIBUTION STATEMENT (of this Report)

Approved for public release; distribution unlimited.

17. DISTRIBUTION STATEMENT (of the abstract entered in Block 20, if different from Report)

18. SUPPLEMENTARY NOTES

19. KEY WORDS (Continue on reverse side if necessary and identify by block number)

| | |
|---|---|
| Air-sea Interaction | Wind Mixing |
| Hurricane Model | Advection |
| Ocean Model | |
| Convective Mixing | |

20. ABSTRACT (Continue on reverse side if necessary and identify by block number)

A layer-ocean model was developed based on the mixed layer models of Kraus and Turner (1967) and Denman (1972). The ocean model was coupled to Pearson's (1972) time varying, symmetrical-stationary hurricane model which was based on a model proposed by Riehl (1963), and in which the air-sea interaction was specified by Cardone's (1969) extension of Blackadar's (1965) two-layer, baroclinic boundary layer model. Time-dependent solutions

DD FORM 1 JAN 73 1473 EDITION OF 1 NOV 65 IS OBSOLETE
(Page 1) S/N 0102-014-6601

for ocean mixed layer depth and temperature were obtained in response to interaction with the atmospheric model. Solutions indicated that the interaction between entrainment mixing and upwelling was most important in changing mixed layer depth and temperature. Radiational effects, internal waves, turbulent scale energy dissipation, and large-scale ocean currents were not included in the present ocean model.

Thesis
F685
c.1
145936
Fraim
Oceanic thermal response to a time-dependent hurricane model.